2011

Statistics in asteroseismology: evaluating confidence in stellar model fits

Erik Stewart Johnson
Iowa State University

Statistics in asteroseismology:

Evaluating confidence in stellar model fits

by

Erik Stewart Johnson

A thesis submitted to the graduate faculty

in partial fulfillment of the requirements for the degree of

MASTER OF SCIENCE

Major: Astrophysics

Program of Study Committee:
Steven D. Kawaler, Major Professor
Lee Anne Willson
John Lajoie
Xiaoqing Wu

Iowa State University

Ames, Iowa

2011

DEDICATION

This thesis is dedicated to everyone who has supported me throughout my research. I thank my family for their support in myriad aspects over my many years of school; their faith in my abilities has never wavered. I cannot fathom how different this period of my life would have been without Susan. I cherished her presence as I completed this work.

TABLE OF CONTENTS

LIST OF TABLES

LIST OF FIGURES

ACKNOWLEDGEMENTS

Rare is the publication that is written without input. From the onset of my graduate study Prof. Steven D. Kawaler has shown himself to be a genial guide, pleasantly encouraging me through every step of the process. His influence is seen throughout this work. I also truly appreciate the contribution to this thesis made by my committee members: Prof. Lee Anne Willson, Prof. John Lajoie, and Prof. Xiaoqing Wu.

ABSTRACT

We evaluate techniques presently used to match slates of stellar evolution models to asteroseismic observations by using numeric simulations of the model fits with randomly generated numbers. Measuring the quality of the fit between a simulated model and the star by a raw χ^2 shows how well a reported model fit to a given star compares to a distribution of random model fits to the same star. The distribution of χ^2 between "models" and simulated pulsations exhibits the behavior of a log-normal distribution, which suggests a link between the distribution and an analytic solution. Since the shape of the distribution strongly depends on the peculiar distribution of modes within the simulations, there appears to be no universal analytic quality-of-fit criterion, so evaluating seismic model fits must be done on a case-by-case basis.

We also perform numeric simulations to determine the validity of spacings between pulsations by comparing the spacing between the observed modes of a given star to those between 10^6 sets of random numbers using the Q parameter of the Kolmogorov-Smirnov test. The observed periods in GD 358 and PG 1159–035 outperform these numeric simulations and validate their perceived spacings, while there is little support for spacings in PG 1219+534 or PG 0014+067. The best period spacing in BPM 37098 is marginally significant. The observed frequencies of η Boötis outstrip random sets with an equal number of modes, but the modes are selectively chosen by the investigators from over 70 detected periodicities. When choosing the random data from sets of 70 values, the observed modes' spacings are reproducible by at least 2% of the random sets. Comparing asteroseismic data to random numbers statistically gauge the prominence of any possible spacing which removes another element of bias from asteroseismic analysis.

CHAPTER 1. INTRODUCTION: SYSTEMATICS OF ASTEROSEISMOLOGY

The field of asteroseismology, like its prefix-less analogue on Earth, focuses on the propagation of waves through stars. Astrophysicists observe effects of these waves in luminosity variations and shifts in radial velocity (Brown & Gilliland , 1994). However, the signals in radial velocity are easier to detect with the Sun in the field of helioseismology. The observational effects imply normal modes of oscillation and each mode contains information about the interior stellar structure. Unambiguously measuring the pulsation frequencies requires long, uninterrupted runs of data, which are increasingly available with space-based instruments such as *Kepler* (Koch *et al.* , 2010). Ground-based efforts also produce some useful results (Winget *et al.* , 1994).

1.1 Nonradial pulsations

A prototypical light curve with multiple pulsation modes is displayed in Figure 1.1. The

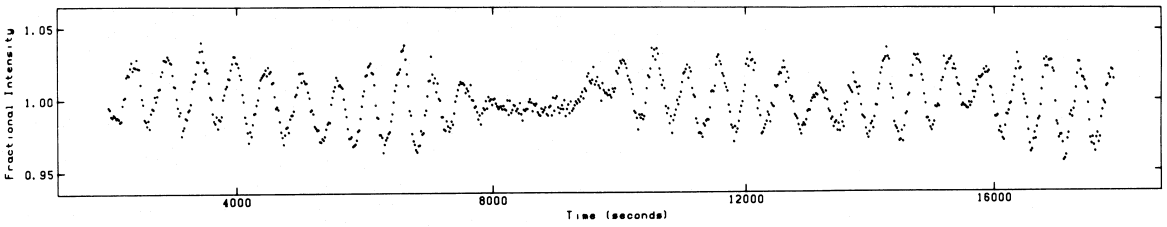

Figure 1.1 A light curve of PG 1159–035 reprinted from Winget *et al.* (1985).

subject of the data collection is PG 1159–035 (hereafter abbreviated as PG 1159), a white

dwarf which has received much attention. This Figure originally appears in Winget *et al.* (1985) along with Figure 1.2, which shows the power spectrum for the same data.

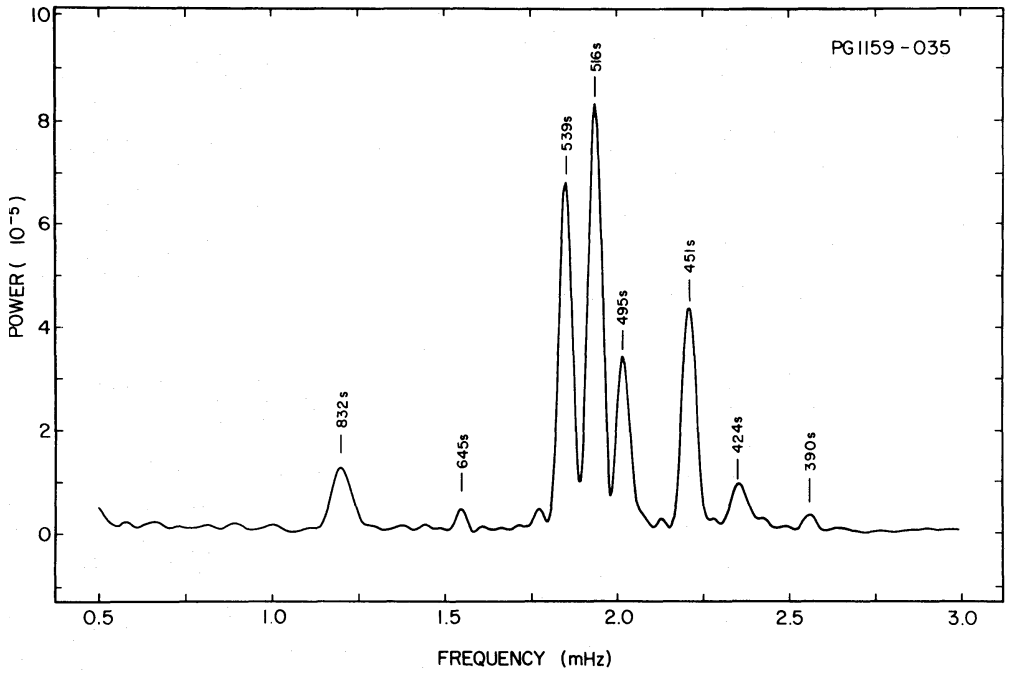

Figure 1.2 The Fourier transform for the light curve in Figure 1.1, also reprinted from Winget *et al.* (1985).

The power spectrum in Figure 1.2 contains eight peaks whose periods correspond to non-radial pulsations with high order of radial wavenumber, n. They involve wave motions in radial as well as horizontal directions. The horizontal oscillations can be decomposed into modes characterized by spherical harmonics with spherical degree ℓ and azimuthal order m (Gautschy & Saio 1995). Two distinct types of pulsation exist, distinguished by their restoring forces: p-modes are oscillations driven by pressure, and g-modes have buoyancy act as a restoring force. The p-modes have periods shorter than the dynamical time scale,

$$\tau_{\rm dyn} = \sqrt{R^3/GM} \ , \tag{1.1}$$

which is roughly an hour for the Sun. They are found in the Sun's spectrum and we also see solar-like p-modes in many main sequence stars via photometry with *Kepler* (Gilliland *et al.* , 2010). The g-modes are characterized by much longer periods than the dynamical time scale

and are more prominent in white dwarfs, but are confined beneath the convective zone in main sequence stars like the Sun.

1.2 Stellar modeling

To find a stellar model that adequately matches the seismic observations astronomers must explore a large grid of model parameters. Using spectroscopy to detect a sufficient number of modes, researchers can judiciously constrain a star's intrinsic properties, including composition, surface temperature, and other global parameters. They can greatly reduce the number of candidate models by attempting to match known pulsations with those present in the stellar models constrained via spectroscopy.

Over a million pulsation modes have been observed in the Sun, but sheer distance and the Sun's presence prevent observers from detecting the same magnitude of modes in other stars. Oscillations observed in these stars often have high radial order, i.e. $n \gg \ell$, and the mode characteristics simplify in a useful way. Tassoul (1980) used asymptotic analysis of high-order overtones to find relationships between successive modes,

$$\sigma_{n,\ell} \approx (n + \ell/2)\sigma_0 \ , \tag{1.2}$$

and

$$\Pi_{n,\ell} \approx n\frac{\Pi_0}{\sqrt{\ell(\ell+1)}} \ . \tag{1.3}$$

Equation 1.2 is valid for p-modes, shows that frequencies for radial overtones, $\sigma_{n,\ell}$, are equally spaced for larger values of the radial wavenumber, n. Equation 1.3, valid for g-modes, indicates that periods for radial overtones, $\Pi_{n,\ell}$, are equally spaced for larger values of n. The spacing parameters, σ_0 for frequency and Π_0 for period, are global in that they are integral quantities,

$$\sigma_0 = \pi \left[\int_0^R \frac{dr}{c_s}\right]^{-1} \ , \tag{1.4}$$

and

$$\Pi_0 = 2\pi^2 \left[\int_0^R \frac{N}{r}\, dr\right]^{-1} \ . \tag{1.5}$$

In Equation 1.4, c_s is the local sound speed for the star, so the integral shown calculates the sound travel time between the center and the surface. Since the frequency parameter is only dependent on the sound speed, c_s, σ_0 correlates with the mean density of the star. The period parameter is dependent on the Brunt-Väisälä frequency, N, implying the degree of temperature and density stratification through the star. Figure 1.3 displays a schematic of a power spectrum with equally spaced frequency peaks as an example of this characteristic.

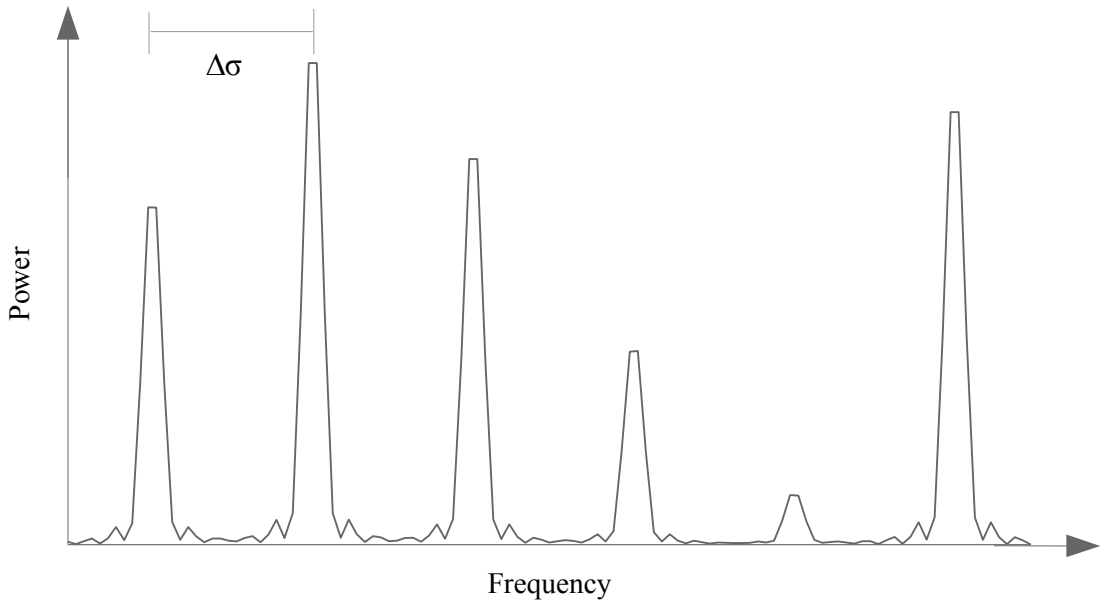

Figure 1.3 A schematic of a power spectrum containing peaks with equal frequency spacing, $\Delta\sigma$.

Constraining an intrinsic parameter like surface gravity reduces the number of variables of stellar constitution and greatly improves the accuracy in stellar modeling. Limiting the range of models allows astrophysicists to hone their understanding of that star in particular and stellar processes in general. Space-based instruments improve continuous observation capabilities and remove observational uncertainties for pulsation modes. Researchers are able to find hundreds of modes in nearby stars, and must employ methods with little to no bias to find the most appropriate stellar model or to find legitimate spacings. This requires rigorous statistical analysis to judge the quality of model fittings and mode spacings.

1.3 Hypothesis

A number of statistical procedures exist to judge the accuracy of a stellar model fit to the pulsation frequencies, along with additional techniques which evaluate candidate spacings perceived in observational data. These methods usually require a selection of data, i.e. the list of identified modes, and omit the associated amplitudes for these modes. We will utilize these methods to test random sets of data with no significant spacings impressed on them a priori. Comparing the test results of sets of pulsation modes to a large number of random sets will allow us to determine the significance of a test performance for data from a certain star. By submitting the random numbers to the same statistics, we may bolster the claims of successful stellar models by showing their results are not attainable by chance. This would put another tool in place to verify model frequencies and mode spacings, refining our understanding of stellar structure.

CHAPTER 2. DIRECT MODELING OF FREQUENCIES

We improve the quality of stellar models by adjusting them to fit all observed pulsations, since this takes advantage of the sensitivity of the oscillation frequencies to the interiors of the stars. However, no standard exists to sift through the multitude of models and retrieve the model which best reproduces the frequencies while matching the other observed constraints within their uncertainties. Thus, researchers employ idiosyncratic methods for testing the validity of their models.

2.1 Asteroseismic observations of η Boötis

The work on the G0 IV star η Boötis (hereafter abbreviated as η Boo) published by Guenther *et al.* (2005) is one such example. The left-hand panel in Figure 2.1, presenting the amplitude spectrum produced by observations from the *MOST* (*Microvariability and Oscillations of Stars*) satellite, is reprinted from Guenther *et al.* (2005). The spectrum range is limited to the region where they expect to find nonradial p-mode oscillations, which corroborates with previous studies of η Boo (Kjeldsen *et al.* , 2003). Guenther *et al.* (2005) use a statistical routine to determine the significant amplitude peaks and produce the significance spectrum shown in the right-hand panel in Figure 2.1.

From there, they present the peak frequencies, ν with $2\pi\nu = \sigma$, on an échelle diagram by dividing the frequency spectrum into segments of length $\Delta\nu$, called the folding frequency, and stacking each segment above the previous one (Grec *et al.* 1983, Bedding & Kjeldsen 2010). A frequency peak's position on the abscissa is determined by its frequency modulo $\Delta\nu$. Modes exhibiting a spacing equal to the folding frequency fall on a vertical line. Guenther *et al.* (2005) construct the modified échelle diagram reprinted in Figure 2.2 with a folding

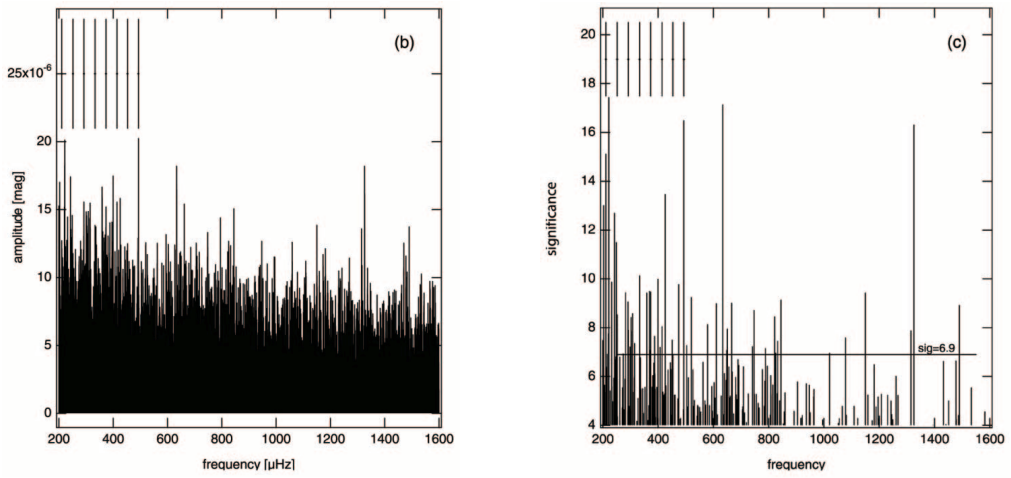

Figure 2.1 Left: the amplitude spectrum of η Boötis reprinted from Guenther *et al.* (2005). Right: the significance spectrum of η Boötis reprinted from the same publication.

frequency constrained to 40 μHz in an effort to match the results published by Kjeldsen *et al.* (2003). The frequency peaks are presented as points and the ordinate continuously shows the frequency of each peak. Figure 2.2 also includes modes identified by previous studies of η Boo, lending credence to a 40 μHz spacing for p-modes as predicted from modeling. They single out these potential p-modes for further study by indicating them with the double circles in the Figure and labelling them as *MOST* modes 1 through 12.

2.2 χ^2 Testing

Guenther *et al.* (2005) then utilize a procedure to find the model containing the closest representations of the *MOST* modes. After constraining the intrinsic properties through other analyses, they construct a grid of 300 000 models with varying metallicities, masses, and ages. They subject the closest modes between the model and the *MOST* selection to a reduced χ^2 test,

$$\chi^2 = \frac{1}{N}\sum_{i=1}^{N}\frac{\left(\nu_{\mathrm{obs},i} - \nu_{\mathrm{mod},i}\right)^2}{\sigma^2_{\mathrm{obs},i} + \sigma^2_{\mathrm{mod},i}} \ . \tag{2.1}$$

Using the χ^2 allows the team to narrow the range of acceptable models as evidenced by Figure 2.3 reprinted from Guenther *et al.* (2005). The Figure presents χ^2 for models with

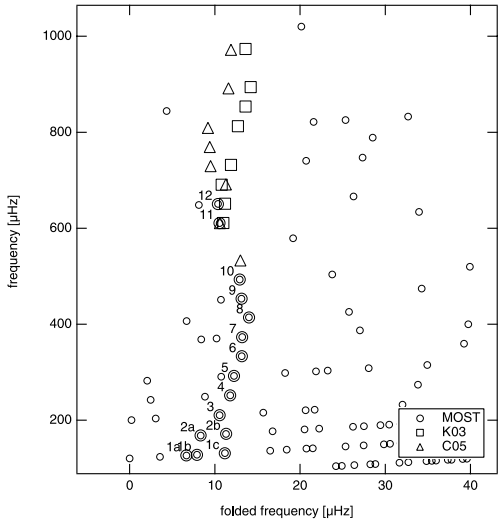

Figure 2.2 An échelle diagram reprinted from Guenther *et al.* (2005) displaying the peaks in the significance spectrum of η Boötis. The double-circled data points are labelled by the original publication as possible p-modes.

hydrogen mass fraction $X = 0.71$ and metallicity $Z = 0.04$. The only models whose χ^2 lie below a threshold of 4.0 are on a nearly two-dimensional sheet with a limited range of evolutionary age for a given mass. A χ^2 of 4.0 implies an average deviation of $2\,\sigma$ ($\sim$0.4 μHz) between the frequencies from the model and observations.

The minimum of the plot in Figure 2.3 corresponds to the parameters of the best model against the *MOST* modes in Guenther *et al.* (2005). They test multiple combinations of *MOST* frequencies with the grid of models and also combine the list of *MOST* frequencies with modes identified by Kjeldsen *et al.* (2003). They achieve similar results by testing the χ^2, but none are as good as using the eight mode set, *MOST* 3–10.

The χ^2 method successfully limits the range of acceptable model properties and outputs a number of models whose χ^2 fall at the minimum for their composition, including one model which is recognized for having the lowest χ^2 overall. However, being deemed "best in show" assumes that most of the fits are good, i.e. better than the average set of numbers can attain. The quality of the χ^2 do not improve with additional modes and the promising results come at the expense of omitting about 50 modes of comparable significance. Cherry-picking modes

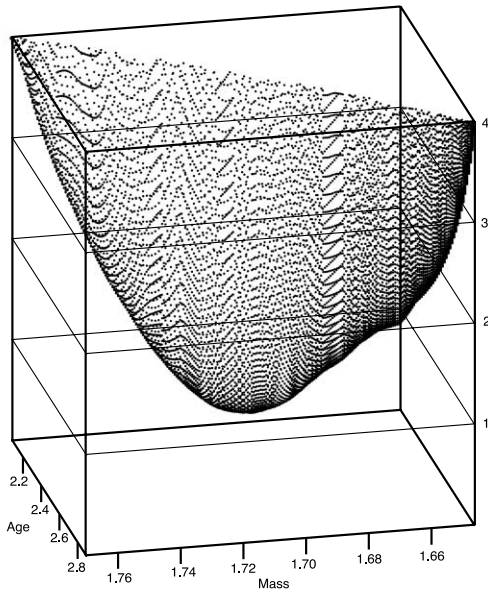

Figure 2.3 A plot of the χ^2 between the models of η Boötis and the observed frequencies as a function of mass ($M_\odot$) and age (Gyr) with $Z = 0.04$ and $X = 0.71$. It is reprinted from Guenther *et al.* (2005).

with convenient frequencies contradicts the aim of using satellites to acquire as much useful data as possible.

2.3 Simulation of observations and models

All stellar models incorporate well-determined physics, e.g. equations of state or reaction rates, with observational constraints, e.g. L, $T_{\rm eff}$, etc., that are particular to the star being studied. Therefore, the physics of stars constrain the expected pulsation frequencies, and observed frequencies refine the input physics. When we focus on the statistics, relatively simple approximations are preferable and should be used in lieu of complex stellar models. If random numbers chosen over the same range representing "observed" or "modeled" frequencies outperform the statistical significances produced by real models, then those models are not meaningfully constraining the physics.

Testing the statistics can be done by simply generating random modes over the proper

range, both for the "target" observations and for the "models." We use the random number generator, ran2, published in Press *et al.* (1992) for this purpose. While any set of modes may be tested with this simulation of modeling, their performance shall be compared to sets which do not contain "real" data, e.g. a set of numbers evenly spaced or a randomly generated set of modes. For the first simulation the "star" has a set of "modes," a_N, selected over a given range. Each set of "modeled" modes, b_N, were produced in the same manner. The version of Hoare's quicksort algorithm presented in Kernighan & Ritchie (1988) arranges the sets in ascending order. As in Guenther *et al.* (2005), the χ^2 tests the deviations between a_i and b_i, $i = 1 \ldots N$. However, the χ^2 used for the simulations is raw, i.e. the model and observational uncertainties are omitted,

$$\chi^2 = \sum_{i=0}^{N-1} (a_i - b_i)^2 \ . \tag{2.2}$$

For comparison, the reduced χ^2 applied by Guenther *et al.* (2005) is

$$\chi^2_{\mathrm{reduced}} = \frac{1}{N} \sum_{i=0}^{N-1} \frac{(a_i - b_i)^2}{\sigma^2_{\mathrm{obs},\,i} + \sigma^2_{\mathrm{mod},\,i}} \ . \tag{2.3}$$

The observational uncertainty, $\sigma_{\mathrm{obs},\,i}$, is estimated at $0.4\,\mu$Hz for *MOST*. The model uncertainty, $\sigma_{\mathrm{mod},\,i}$, is estimated from models of the Sun to be an order of magnitude smaller than $\sigma_{\mathrm{obs},\,i}$ so it does not significantly affect $\chi^2_{\mathrm{reduced}}$.

We are looking for a general description rather than trying to match the analysis of Guenther *et al.* (2005), so the first simulation generates numbers over a normalized range of 1. The eight "observed" values are compared to 10 000 sets of "models" of equal size. The distribution of χ^2 for the "star"–"model" comparison is displayed in Figure 2.4 which also shows a log-normal distribution function fitted with the statistical software JMP. A set with the behavior of a log-normal distribution exhibits the characteristics of a normal distribution when the abscissa is a logarithmic scale. The probability density function for this distribution,

$$\mathrm{pdf}(x; \mu, \sigma) = \frac{1}{x\,\sigma\sqrt{2\pi}} \exp - \left[\frac{\ln(x) - \mu}{\sqrt{2}\sigma}\right]^2 \ , \tag{2.4}$$

contains two constants which define the scale and shape of the distribution: μ and σ. These constants are respectively the mean and the standard deviation of the natural logarithm of the distribution.

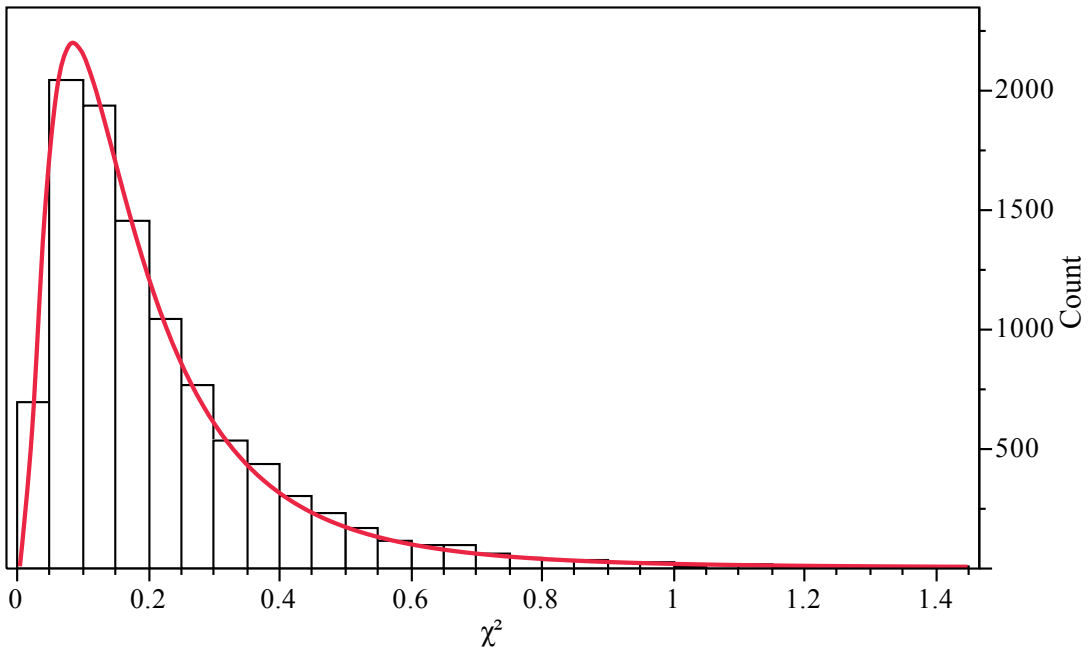

Figure 2.4 The distribution of the χ^2 for 10 000 "model" sets matched with the initial "observed" set. The curve represents the fitted log-normal distribution function.

With a lower value of σ, the peak is more pronounced, and μ affects the scale of the range of values. For this distribution, μ is estimated by JMP at -1.843 and σ at 0.7751. If the distribution is an ideal log-normal distribution, the mean and median may also be used to determine μ and σ via

$$\mu = \ln(\text{median}) \ , \tag{2.5}$$

and

$$\sigma = \sqrt{2 \ln \left(\frac{\text{mean}}{\text{median}} \right)} \ , \tag{2.6}$$

respectively. In this simulation, the distribution has a mean of 0.2103 and a median of 0.1602, which imply a μ of -1.831 and σ of 0.7371, both within 5% of the JMP estimates.

While a log-normal distribution appears to fit the simulation well, a goodness-of-fit test offers a proper gauge of the quality of the fit. The JMP-estimated values for μ and σ may contribute to a better result for the probability density function, but the function should incorporate the simulation-dependent parameters in Equations 2.5 and 2.6 so outliers will not

be effectively ignored.

2.4 The Kolmogorov-Smirnov test

To determine the goodness-of-fit between the probability density function and the simulation, we employ the Kolmogorov-Smirnov (hereafter K–S) test. The K–S test utilizes the cumulative distribution function (hereafter CDF) which evaluates the fraction of a set below a given value. Since the set of χ^2 is sorted in the simulation, the function must only identify the highest element smaller than the given value, and the element's position in the array leads to the outputted fraction. The CDF for the log-normal distribution is derived by integrating Equation 2.4 from zero to a given value of x,

$$\mathrm{cdf}(x;\mu,\sigma) = \frac{1}{2} + \frac{1}{2} erf\left[\frac{\ln(x)-\mu}{\sigma\sqrt{2}}\right] \ . \tag{2.7}$$

The basic statistic for the K–S test is Kolmogorov's D and measures the maximum difference between the CDFs of two sets over their ranges. Figure 2.5 displays the CDF for both the distribution of χ^2 and the fitted log-normal distribution for the simulation of the goodness-of-fit to a set of frequencies for a large number of "stellar models." The blue line in Figure 2.5 represents the ongoing value of D, i.e. the maximum displacement observed between the two curves. The maximum deviation occurs when $\chi^2 = 0.292$ and the displacement is 0.0159, implying there is never more than a 1.59% difference between the CDF of each distribution.

The significance of the observed D may be calculated using the following formula for Q reprinted from Press *et al.* (1992),

$$Q(\lambda) = 2\sum_{j=1}^{\infty}(-1)^{j-1}\, e^{-2j^2\lambda^2} \ . \tag{2.8}$$

Equation 2.8 allows us to determine the probability that D is lower than we observe by evaluating Q for the following value of λ,

$$\mathrm{Probability}(D > \mathrm{observed}) = Q\left(\left[\sqrt{N_e} + 0.12 + 0.11/\sqrt{N_e}\right] D\right) \ . \tag{2.9}$$

N_e refers to the number of elements in the distribution being tested, which is equal in our case to the number of models. For the statistical test, we set the null hypothesis, H_0, that the

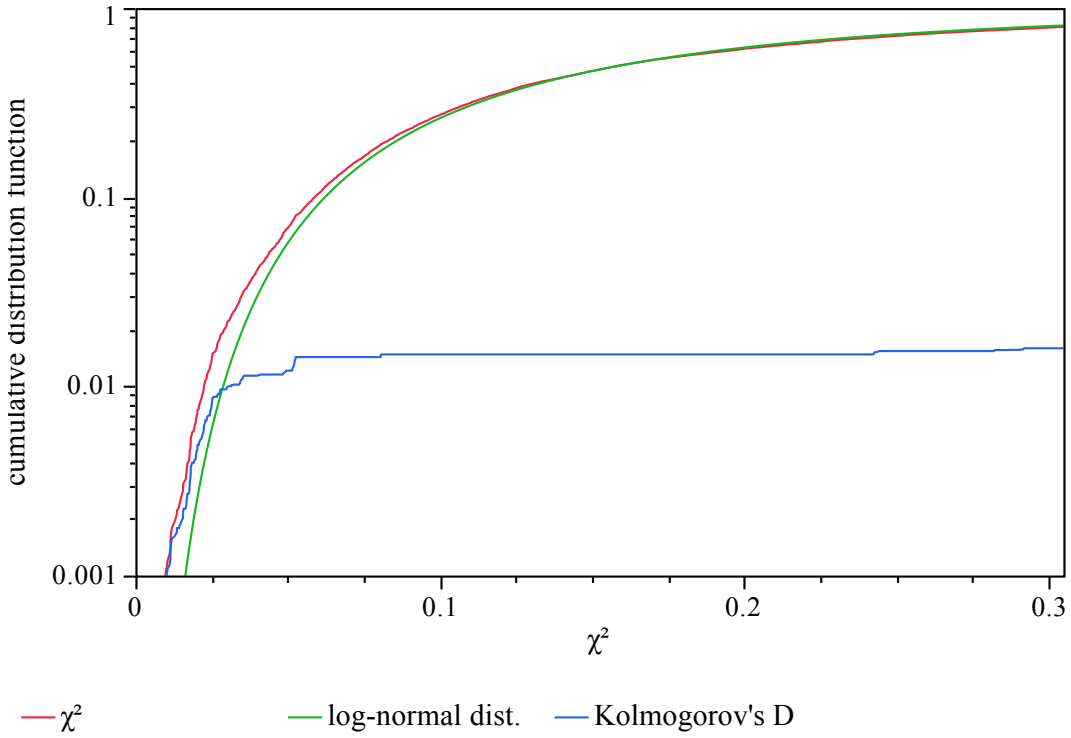

Figure 2.5 The cumulative distribution function (CDF) for both the set of χ^2 produced and the fitted log-normal distribution based on the simulation. Kolmogorov's D shows the maximum deviation between the CDF of each distribution and reaches a maximum value of 0.0159 when $\chi^2 = 0.292$.

two distributions are the same. In this case, a lower value of Q indicates a greater difference between the two distributions. We may set a significance level to disprove the null hypothesis for small values of Q. In the case of the simulation, Q is 0.0127, meaning that we could reject H_0 for a 5% significance, but would fail to reject H_0 for 1% or smaller. If such results are typical, there may exist an analytical solution for the distribution based on the range and number of "observed" modes.

2.5 Deriving an analytic solution to the χ^2 distribution

2.5.1 Additional modes in the set

If there exists an analytic way of computing the parameters of the distribution as a function of the number of modes we try to match with the models, the analytical method would present itself as N, the number of modes of the "star," changes. The range of "observations" and "models" is still 1, and 10 000 simulated models were used. The random number generator is reset at the start of each simulation to preserve repeatable results. This limits the "observed" modes to having the same numbers, but multiple random sets will be tested later. Figure 2.6 shows the distribution of χ^2 for a simulated star with eight to twelve modes.

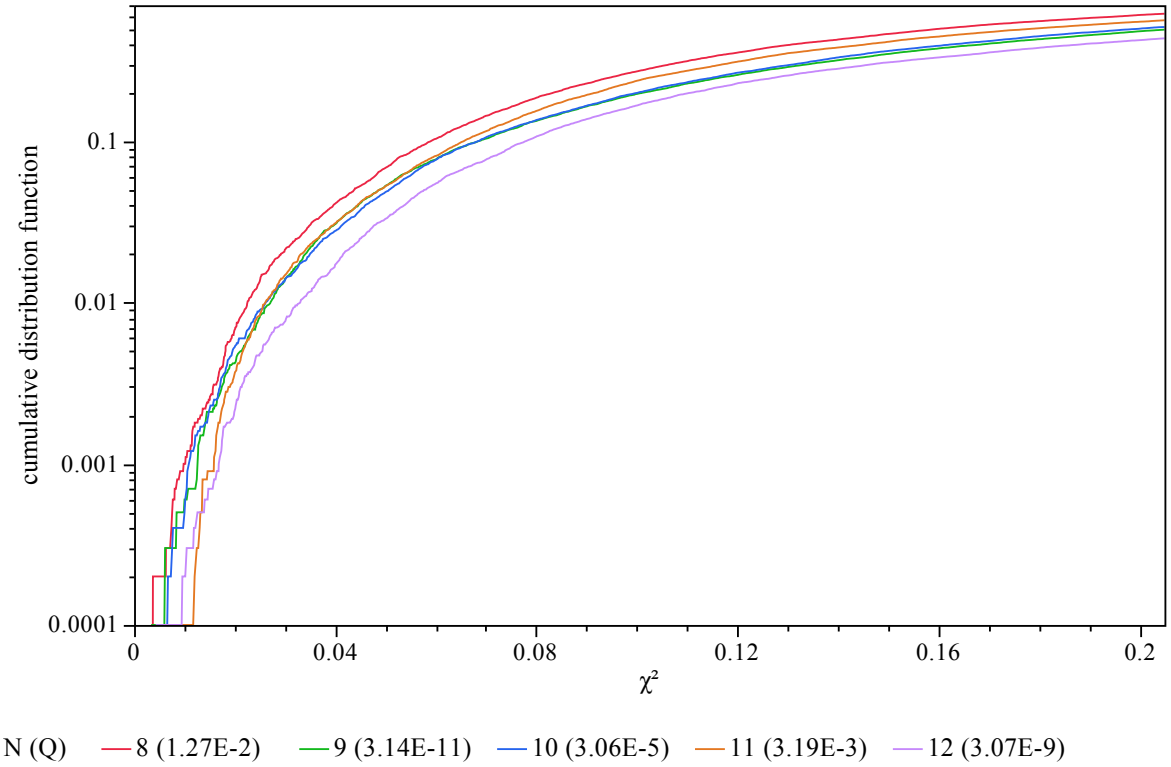

Figure 2.6 The CDFs of the distribution of χ^2 between 10 000 "models" and a set of between eight and twelve "observed" modes. The significance Q of the distribution's fit to a log-normal distribution is given in parentheses.

Generally, the raw χ^2 are higher with more modes, meaning that the CDF is lower for the distribution for higher values of χ^2. However, there is significant overlap between the CDF curves, and the CDF for the simulation of matching eleven modes is higher than those for nine or modes. The distributions and the CDF for each may be affected by each mode added to the simulated set of frequencies, specifically pertaining to their placement within the set. Table 2.1 shows the twelve modes of the "star," with the first eight arranged in increasing order. We examine the effects of including the last four modes in further detail.

Table 2.1 The first twelve modes of the simulated star. The first eight are sorted in increasing order.

1	0.09347	**2**	0.1959	**3**	0.2534	**4**	0.2854
5	0.4630	**6**	0.6085	**7**	0.9034	**8**	0.9390
9	0.1272	**10**	0.4159	**11**	0.5337	**12**	0.1074

Since we are using a raw χ^2, we are not reducing the value by dividing by the number of modes. With more modes there are more deviations, so the χ^2 is likely to increase with each added mode. The range of the eight modes is 0.845 with an average spacing of 0.106 between each mode. The ninth mode, 0.127, lies within the same range and in relative proximity to the first mode, 0.0935. Recall that these "models" only have the same number of modes as the simulated star, and that matching does not currently consist of determining the closest fitting mode for each observed frequency. The two sets of modes are paired off in order of increasing frequency instead. Having to fit "models" to two modes with little spacing between them increases the average χ^2 of the simulation which shifts the CDF in Figure 2.1 to the right.

The tenth simulated frequency, 0.4159, is located between modes 4 and 5, which is the second largest gap between the nine modes. Seven of the first ten modes are in the lower half of the range, so the highest χ^2 are generated by simulated models with a disproportionate number of modes in the upper half of the range. However, the deviation between modes above 0.5 and the tenth mode is smaller than between modes 1–4 and 9. This likely contributes to the lack of shift in the distribution from nine modes to ten.

The eleventh mode, 0.5337, fills another gap between modes 5 and 6 and is in the upper half of the range. This improves the distribution of the simulated frequencies by mitigating the deviation from the worst fitting "models" and shifting the upper portion of the CDF to the left. Conversely, a better distribution means the random models whose modes are disproportionately in the lower half of the range do not fit the eleven modes as well as the nine- or ten-mode simulations. Thus, the lower portion of the CDF for the eleven-mode simulations is shifted to the right.

The twelfth mode, 0.1074, lies between modes 1 and 9 which contributes to the existing imbalance of the modes' distribution. If simulated models are similarly imbalanced the deviation between the "models" and the "observed" set remains low or decreases and the χ^2 does the same. However, more well-distributed "models" have higher χ^2. Altogether, this shifts the lower portion of the the CDF to the left and the upper portion to the right relative to the CDF for the eleven-mode χ^2.

A simple and general relationship between the number of modes and the parameters describing a log-normal distribution does not appear to exist. The distribution appears to depend on the particular values for each "observed" set of modes. This is clearly shown by analyzing the contributions of an additional mode to an existing distribution.

2.5.2 The selection of N from a pool of M

If models consist of more modes than the set of modes identified from observations, we must choose the model frequencies which best match those observed. Retaining the best model modes would improve the raw χ^2 and lower the distribution. The desired algorithm would match each observed frequency with its closest model, achieving the minimum χ^2 possible. However, this can lead to a long runtime so the average number of steps in the algorithm needs to be minimized.

Working with the sorted arrays, our first version of the algorithm, trimming, compares the first and lowest observed mode with the first two model modes. If the lower element is a worse fit, it is bypassed and the next model element is then compared to the higher

element. After the maximum number of model modes are bypassed, the remaining modes are automatically matched regardless of the quality of fit. While this method has fewer operations than more sophisticated methods, it suffers from a bias of selecting lower values, and does not achieve the same results working in reverse. For example, Table 2.2 shows the statistics of the distribution of χ^2 when random models are matched to the original simulated star. The eight best modes from the "model" are chosen from a pool of twelve modes, starting from either the lowest or the highest mode. The statistics of the original simulation in §2.3 are also presented for comparison. As expected, the ability to remove some inconvenient modes lowers the distribution of χ^2. Since the distribution is more compact, σ increases and D is not consistently altered by the change. Since the performance by trimming depends on where it originates, a "rejection" algorithm must be more rigorous in finding the best matches.

Table 2.2 The statistics of the χ^2 distributions for 10 000 models matched to a "star" with eight modes ($N = 8$). The trimming algorithm selected the best eight modes of twelve ($M = 12$), beginning with either the lowest or highest mode.

M	mean	median	mode	μ	σ	D	Q
8	0.210	0.160	0.0931	−1.83	0.737	0.0159	1.27×10^{-2}
12 (lowest)	0.0816	0.0539	0.0235	−2.92	0.910	0.0277	4.54×10^{-7}
12 (highest)	0.0641	0.0443	0.0211	−3.12	0.860	0.0110	1.76×10^{-1}

2.5.2.1 Selecting the best differences possible

This method consists of looking at the absolute differences between all modes in the observed star and the models. The differences are stored in an array with $M \times N$ elements, while the identities of the modes that produced each difference are stored in a separate array. The array of differences is quicksorted and the second array containing the mode numbers is correspondingly rearranged. The best modes come from the smallest differences with no bias toward the modes processed first.

Although our second version of the algorithm, trim_abs, works well and is easy to conceive, it uses a great deal more memory and is more time-consuming than trimming. When matching

twelve model modes to an eight-mode star, trim_abs produces two 96-element arrays which must be sorted to find the best modes.

The array may be restricted since each stellar mode can only match with $M - N + 1$ possible modes; e.g. in a twelve-choose-eight situation, the lowest mode cannot line up with the sixth through the twelfth modes in the model. Therefore, the array in our third version of the algorithm, trim_off_n, only needs to have $(M - N + 1) \times N$ elements, e.g. a 40-element array for twelve-choose-eight. While this is a great improvement, the array can be made reasonably smaller.

2.5.2.2 The compromise algorithm, ranking

The general procedure above is intended to find the best fitting model mode for each observed mode, with no more than one observed mode matched with the same model mode. However, the matching procedure may match an observed mode with a far-flung model mode because all nearby model modes have been matched. Figure 2.7 illustrates this plausible phenomenon, where the best remaining choice for observed mode 4 is larger than the model modes matched to modes 5 and 6. In a few cases, the process fails to assign any model mode to match a given observed mode. We have corrected these flaws so the observed modes are matched with the closest model modes available, leading to occasional duplicates.

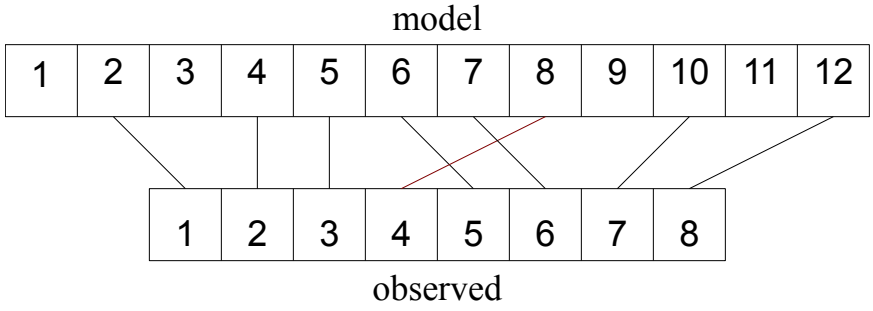

Figure 2.7 A flaw in the procedure used by trim_abs to find the best matching model modes to a set of observed modes. The lines between the two sets indicate the matches, and the red line signifies a mistaken fit for mode 4.

The final version of the algorithm integrates the concepts applied in trimming and trim_abs.

Called ranking, it consists of one-by-one comparisons of all the elements of the arrays to find the smallest absolute difference. The algorithm dispenses with the absolute difference array because the two arrays are already sorted and finding the best possible difference is irrelevant.

Table 2.3 displays the statistical differences between each version of the selection algorithm when simulating 100 stars being matched to 100 000 models each. Each model has eight modes sifted out of a possible twelve. Since the mean and median scale with μ, Table 2.3 only shows the median μ of the 100 distributions, as well as the median values of σ, D, Q and the total runtime (on a 2 GHz Intel Core 2 Duo processor with 1 GB of 667 MHz DDR2 SDRAM) of the operations. In each case, more than half of the 100 simulations produced the minimum value of Q, which is likely because N_e is now 10^5 and Equation 2.8 becomes exponentially smaller with increasing N_e.

Table 2.3 The median statistics and runtime of the three selection algorithms matching 10^5 models to 100 simulated stars.

algorithm	μ	σ	D	Q	runtime
none removed	-1.63	0.699	0.0319	$< 10^{-45}$	$24\,s$
trimming (lowest)	-2.71	0.829	0.0321	$< 10^{-45}$	$36\,s$
trimming (highest)	-2.72	0.840	0.0269	$< 10^{-45}$	$36\,s$
trim_abs	-4.04	0.864	0.0302	$< 10^{-45}$	$250\,s$
trim_off_n	-3.44	1.05	0.042	$< 10^{-45}$	$117\,s$
ranking (lowest)	-4.04	0.864	0.0302	$< 10^{-45}$	$38\,s$
ranking (highest)	-4.04	0.864	0.0302	$< 10^{-45}$	$36\,s$

As intended, statistical performance of ranking is independent of the order of modes. Runtime can still be affected, but that is dependent on the distribution of modes. Since duplicable model modes obviate the need for closest matches, the statistics for the corrected trim_abs are identical to those of ranking, but in 15% of the runtime as seen in Table 2.3. Scaling this simulation up to 10^5 stars with 10^5 models each, the runtime would be about 10.6 hours.

Figure 2.8 shows the distribution of χ^2 for "stars" with eight modes matched to "models" with between eight and twelve modes where the algorithm finds the best matches. The shift in the distributions is dramatic with the mode options that ranking provides and when working with additional modes, the decrease is monotonic. The shape of the distributions is much

sharper, as seen by the increase in σ. As seen in Q, the distributions all behave less like a log-normal distribution when the modes are better matched. Since N_e is unchanged between these curves, the increase may be attributed to the change in D.

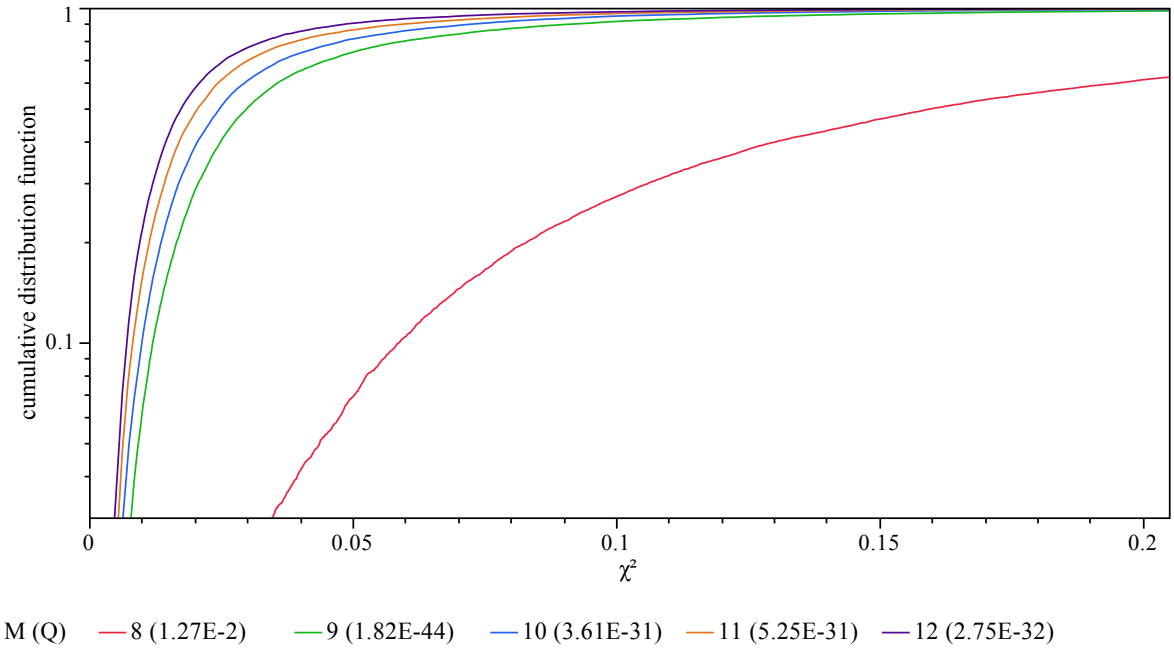

Figure 2.8 The CDF of both the distribution of χ^2 between eight "observed" modes and the closest models. The K–S test statistic Q is listed in parentheses next to the initial number of model modes.

2.5.3 Increasing the number of models

An exorbitant number of "models" can be used in the simulation for a star, but as seen in §2.5.2 computing time must be considered if the program runs take several days. Additionally, if real stellar models are being considered, the time to calculate structure and oscillation frequencies exacerbates the computing problem. Increasing the number of models affects the number and range of outliers, but if the overall distribution is not significantly altered, this potential information may be omitted for the sake of convenience. Figure 2.9 compares the statistics of the simulations as the number of "models" go up by an order of magnitude. The eight-mode "star" from §2.3 is matched with up to 10^7 untrimmed random models, but the

CDF for 10^7 "models" has been subtracted from each CDF in the Figure to better illuminate the variation between the curves. Therefore, the greatest amplitude for a given line is D between that curve and the curve labelled "10^7" in Figure 2.9. Unsurprisingly, 10^6 simulated models achieves the closest result, but an increase in models does not improve D between the CDF and the fitted log-normal distribution. A minimum of 10^4 models may be sufficiently close for future tests, but we implement 10^5 as in §2.5.2.

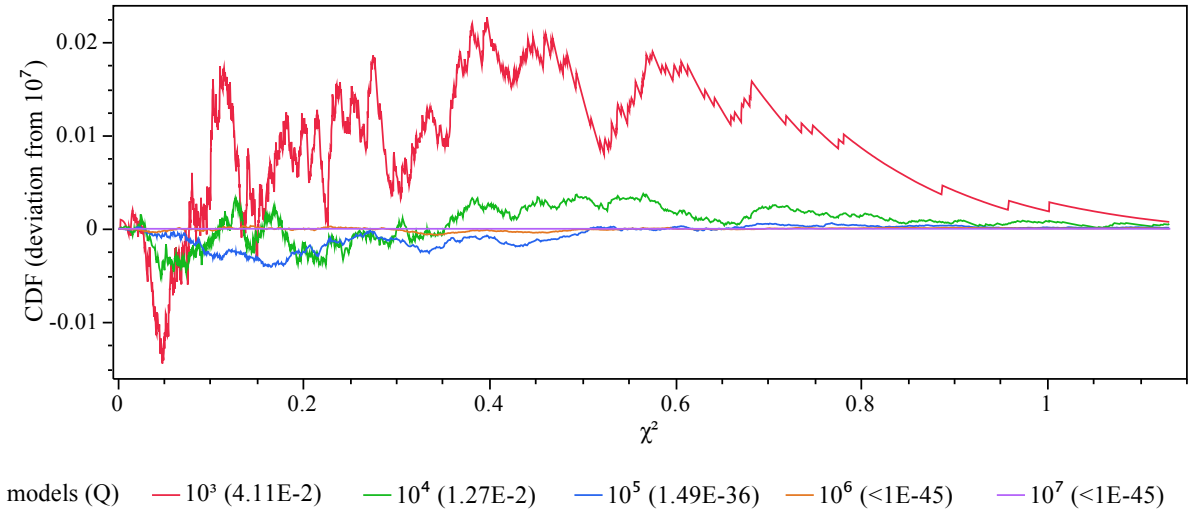

Figure 2.9 Each CDF produced by matching the original simulated star to betwen 10^3 and 10^7 "models" The calculated Q statistic is displayed as well.

2.5.4 Distribution of stars with a distribution of models

Akin to the escalating number of models in §2.5.3, the next phase of testing simulates between 10^2 and 10^6 "stars." Each one has eight "observed" modes and a generated set of 10^5 "models" unique to each. Multiple distributions would be impossible to compare on a single plot, so the accompanying figures compare the statistics of the distributions. Figure 2.10 attempts to shed light on the "meta-statistics," showing the distribution of the means of the distributions of χ^2 produced with each simulated star. In addition to the means, Figure 2.11 presents the distribution of the medians. Like Figure 2.9, the means and medians are compared to the same values found with 10^6 random stars by plotting the deviations. The placement of

the zeroth percentile is outside the range of the plot to allow better focus on the comparison of the 10^{th} and 100^{th} percentiles between the lines. These Figures achieve analogous results to those seen in §2.5.3; 10^4 "stars" would suffice, but 10^5 "stars" are enough of an improvement to justify the time required to complete the simulations.

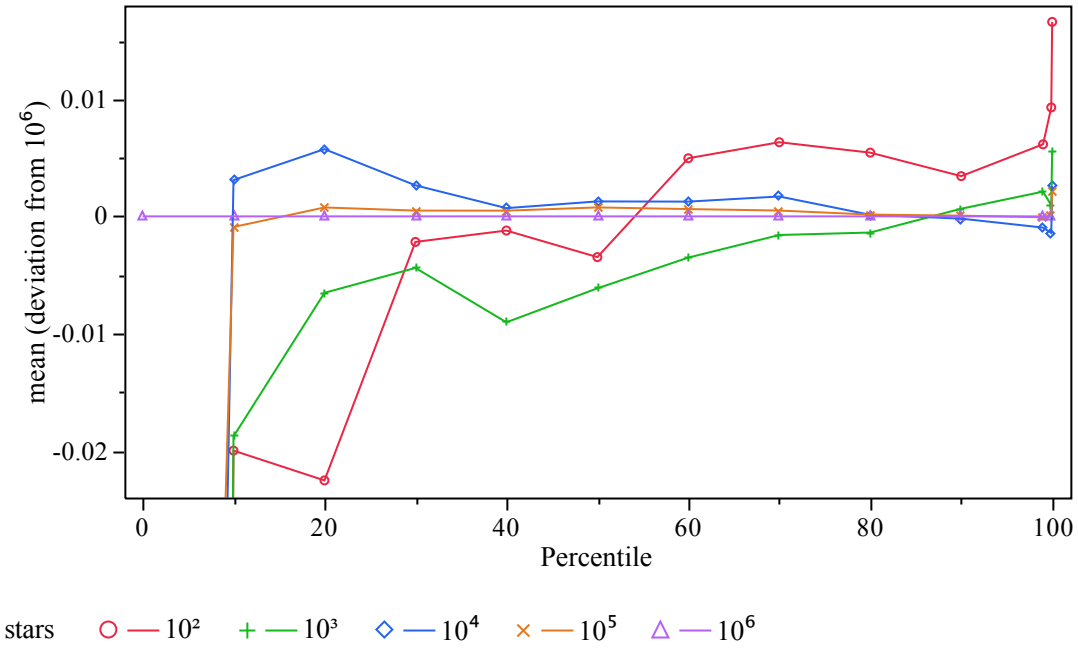

Figure 2.10 The variation of the means of the χ^2 distribution for 10^2–10^6 simulated stars.

2.5.5 Seeking uniformity between distributions

The final simulations run 10^5 stars against 10^5 models apiece. One of the tests uses random stars with between eight and twelve modes, i.e. increasing N, matched to "models" of equal size. The other simulation uses eight-mode stars and models with up to twelve modes, i.e. increasing M, which are trimmed using the ranking algorithm from §2.5.2. Figure 2.12 shows the distribution of medians of the distributions of χ^2 for the simulations with increasing N, and Figure 2.13 displays the analogous statistics for simulations with increasing M.

Keeping the outliers on the graph once again affects the perspective of the rest of the distribution. Thus, the lower panels in Figure 2.12 and Figure 2.13 display only the lower values which accentuates the differences between the distributions over the lower 90%. The

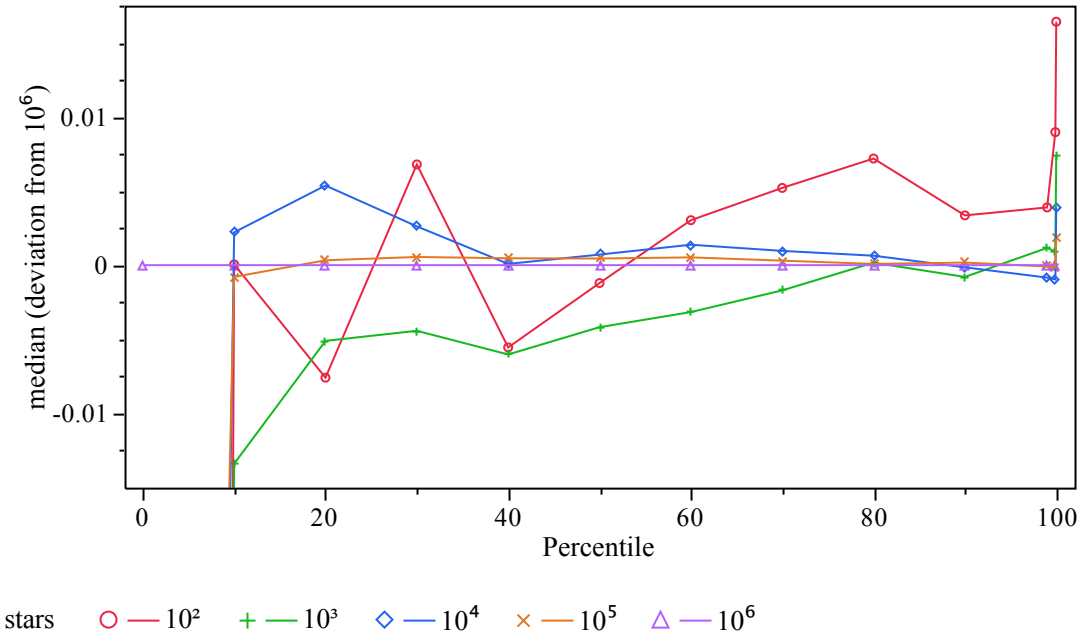

Figure 2.11 The variation of the medians of the χ^2 distribution for 10^2–10^6 simulated stars.

bottom image in Figure 2.12 also has the eight-mode medians at each percentile subtracted from all the curves to further highlight the range of the curves.

The red line in each Figure is the same data; eight-mode "stars" were matched perforce with the eight modes available to them as in the simulation from §2.3. The first simulation performs slightly above average, i.e. lower statistics, compared to the other stars in this distribution. The mean, median and calculated D for the original random star all lie in the 70^{th} percentiles. Since the first simulation is not an outlier, it appears to be a good representative example of a "star" with random modes.

As the number of modes increase the shape of the distribution in Figure 2.12 hardly changes, but the increase is monotonic as the lower portion of the Figure shows. The curves shift more dramatically in Figure 2.13 when the option of choice is presented. However, having additional modes as fodder for ranking drops the curves only slightly further. The shape is consistent between the curves for $m = 9$ to $m = 12$ in Figure 2.13, unlike those seen in Figure 2.12 between $n = 8$ and $n = 12$. Clearly, each simulated star will have a unique χ^2 distribution depending on its frequencies. The vagaries of random modes imply that there is no typical

result for all “stars” in this distribution.

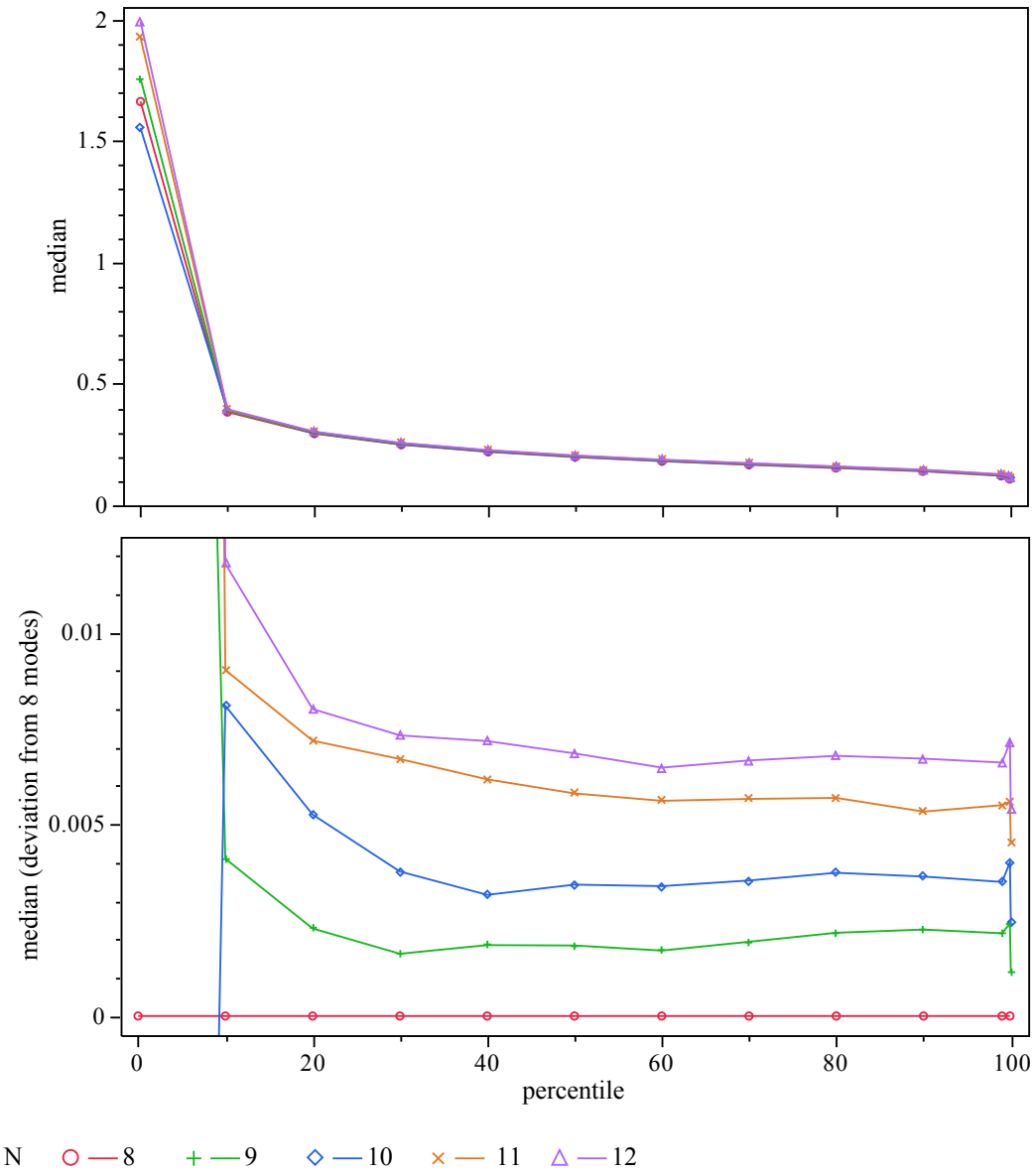

Figure 2.12 Top: The medians of the distributions of χ^2 for 10^5 simulated stars with eight to twelve modes. Bottom: the differences from the eight-mode distribution.

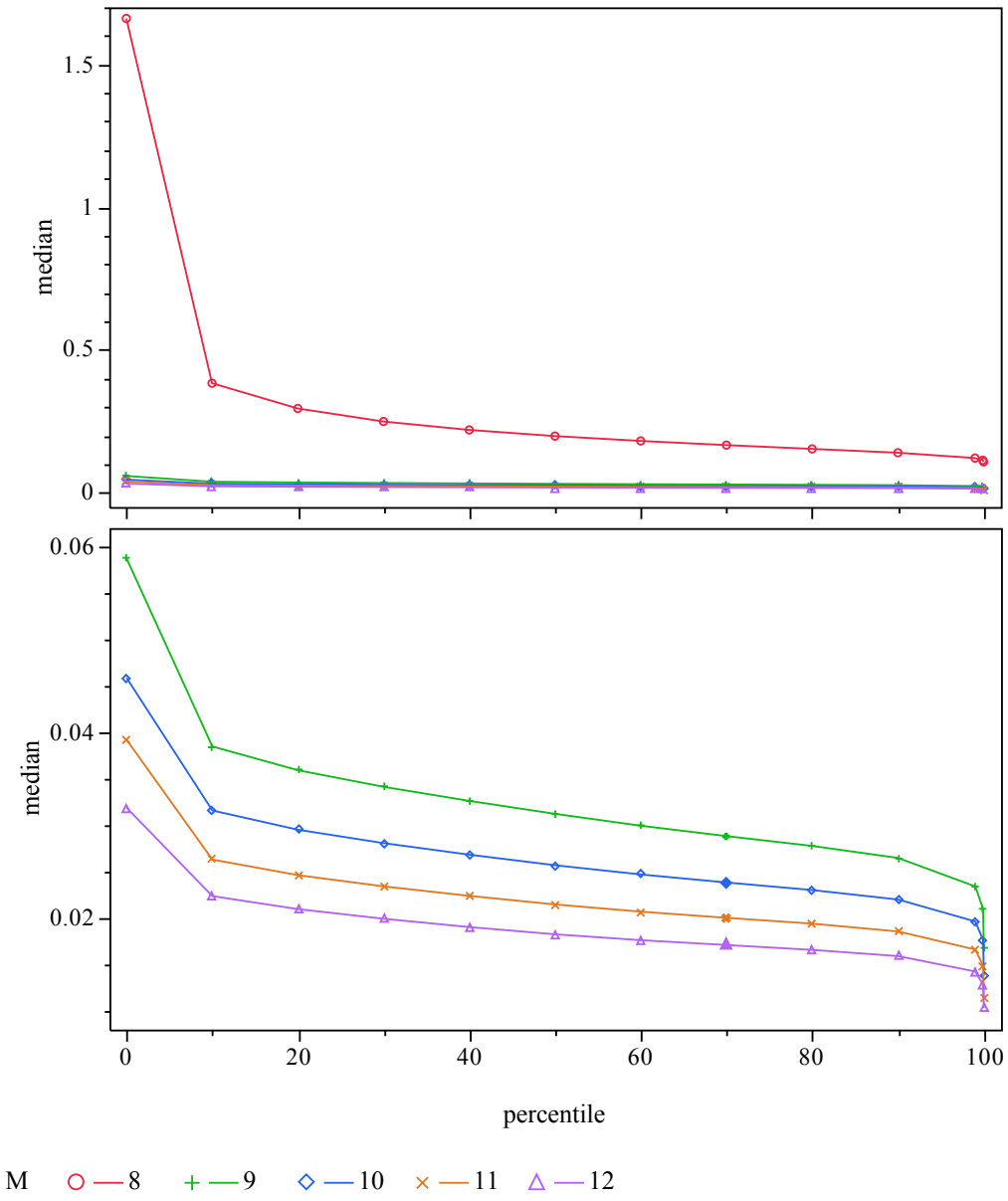

Figure 2.13 Top: The medians of the distribution of χ^2 for 10^5 simulated stars with eight modes against models with up to twelve modes. Bottom: a closer focus on the distributions for nine to twelve modes.

2.6 A sample distribution test using pulsation data

As a test of fitting sets of randomly generated numbers with pulsations identified in the literature, we use BPM 37093, a white dwarf star whose frequencies are reported in Kanaan *et al.* (2005). In an attempt to match the fifteen observed frequencies with up to 100 000 sets of fifteen numbers, we produce the distributions shown in Figure 2.14. The median χ^2 is

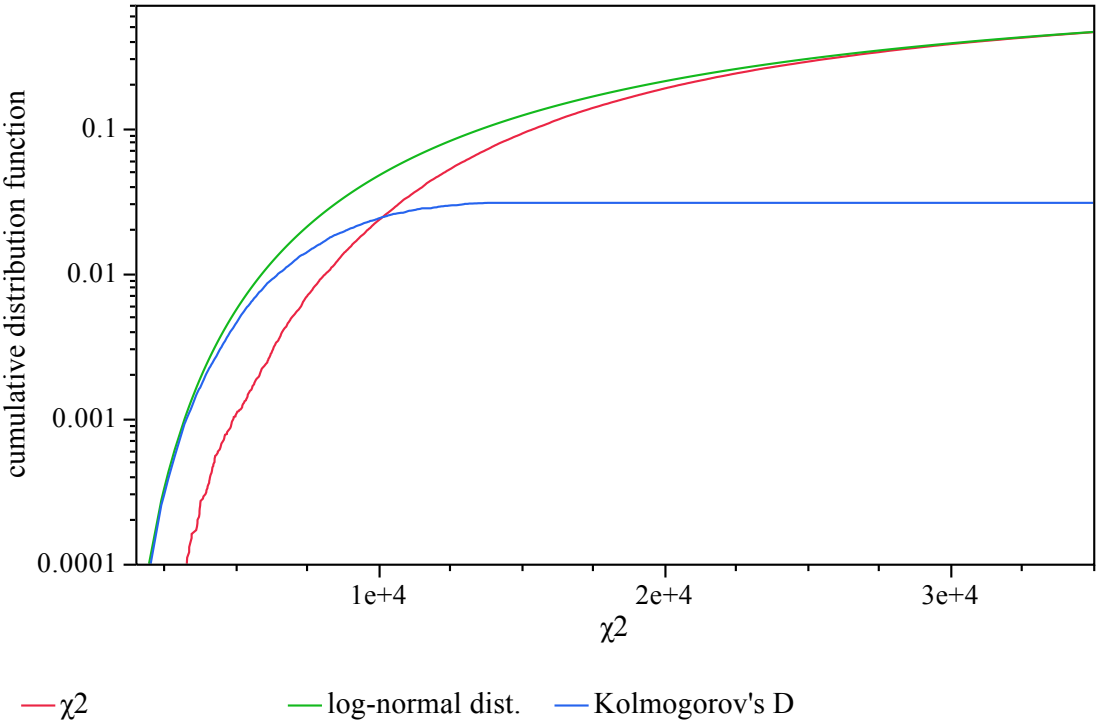

Figure 2.14 The CDF for the distribution of χ^2 of 10^5 simulated models with fifteen modes against the fifteen frequencies of BPM 37093 identified by Kanaan *et al.* (2005). The CDF for the log-normal distribution and the increasing maximum deviation between each CDF are also included. The maximum value of D is 0.0303 when $\chi^2 = 1.38 \times 10^4$.

3.83×10^4 which is outside the range of the plot in Figure 2.14. If the χ^2 were reduced by dividing the number of frequencies, the median χ^2_{reduced} would be 2.55×10^3. The CDF of the distribution never deviates more than 3.03% from the log-normal distribution, but with 10^5 models Q falls below 10^{-45}, so the two distributions appear to be significantly different according to the K–S test. The best raw χ^2 is 1.77×10^3, corresponding to a reduced χ^2 of

1.18×10^2. This is two orders of magnitude worse than what is achieved with well-calibrated stellar models. By comparison, the closest matching model in Kanaan *et al.* (2005) has a root-mean-square (rms) difference between the observed and calculated periods of 1.08 s. An rms difference is the same as the square root of the reduced χ^2 when the uncertainties are omitted, so the minimum reduced χ^2 for the stellar models is 1.17, or a raw χ^2 of 17.5.

In a second attempt, we elect to find the closest model frequencies out of a set of nineteen for the observed modes of BPM 37093. The distribution of these χ^2 are in Figure 2.15 and the statistics for these two distributions may be found in Table 2.4. Due to matching the

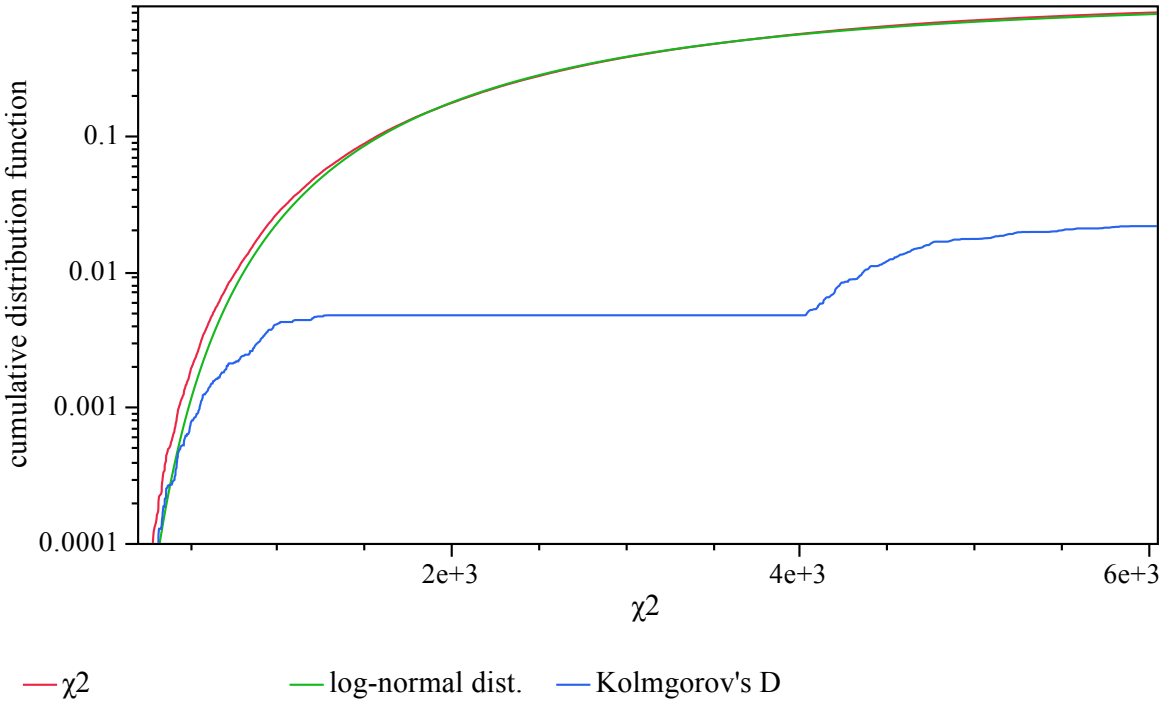

Figure 2.15 The CDF for the distribution of χ^2 of 10^5 simulated models with nineteen modes against the fifteen frequencies of BPM 37093 identified by Kanaan *et al.* (2005). The CDF for the log-normal distribution and the increasing maximum deviation between each CDF are also included. The maximum value of D is 0.0214 when $\chi^2 = 5.90 \times 10^3$.

closest modes, the median of the distribution drops by an order of magnitude to 3.69×10^3, or a reduced χ^2 of 2.46×10^2. The distribution is less than or equal to 2.14% from a log-normal distribution throughout, but the Q is still low enough to reject the null hypothesis that the

Table 2.4 The statistics of distributions of 100 000 models with M frequencies matched to the fifteen modes of BPM 37093.

M	mean	median	mode	μ	σ	D	Q
15	5.282×10^4	3.834×10^4	2.020×10^4	10.55	0.8005	0.03034	$< 10^{-45}$
19	4.556×10^3	3.691×10^3	2.422×10^3	8.214	0.6490	0.02137	4.35×10^{-40}

distributions are the same. Interestingly, the maximum deviation makes a significant jump in Figure 2.15 after the median of the distribution, but D remains lower than the value seen in Figure 2.14. The lowest χ^2 is still quite high: 2.23×10^2 or 14.8 when reduced. This result comes from finding fifteen model modes out of nineteen. If we increase the size of the pool to allow for all the simulated model modes that may be found in a given range, a comparable χ^2 may be within reach.

Since the tests in §2.5.5 only consider eight to twelve modes, we may not use them as a basis for comparison with BPM 37093. We run a fifteen-mode test matching 10 000 simulated stars to 100 000 models each. However, since the range of modes is one we must normalize the frequencies of BPM 37093. We set a range for the modes based on the lowest and highest frequencies, a_0 and a_{n-1} respectively,

$$\text{range} = (a_{N-1} - a_0)\frac{N}{N-1} \ , \tag{2.10}$$

and we set the minimum frequency,

$$\text{minimum} = a_0 - \frac{\text{range}}{2N} \ . \tag{2.11}$$

To reset the minimum to zero and the range to one, we adjust every frequency to the modified frequency, a_i',

$$a_i' = (a_i - \text{minimum})/\text{range} \ . \tag{2.12}$$

Figure 2.16 shows the χ^2 distributions with the normalized frequencies of BPM 37093. Normalizing the frequencies does not affect the shape of the distribution and preserves the calculated σ. The deviation from the log-normal distribution is also unaltered so D and Q are unchanged as well. This is best illustrated by comparing the characteristic jump in the blue

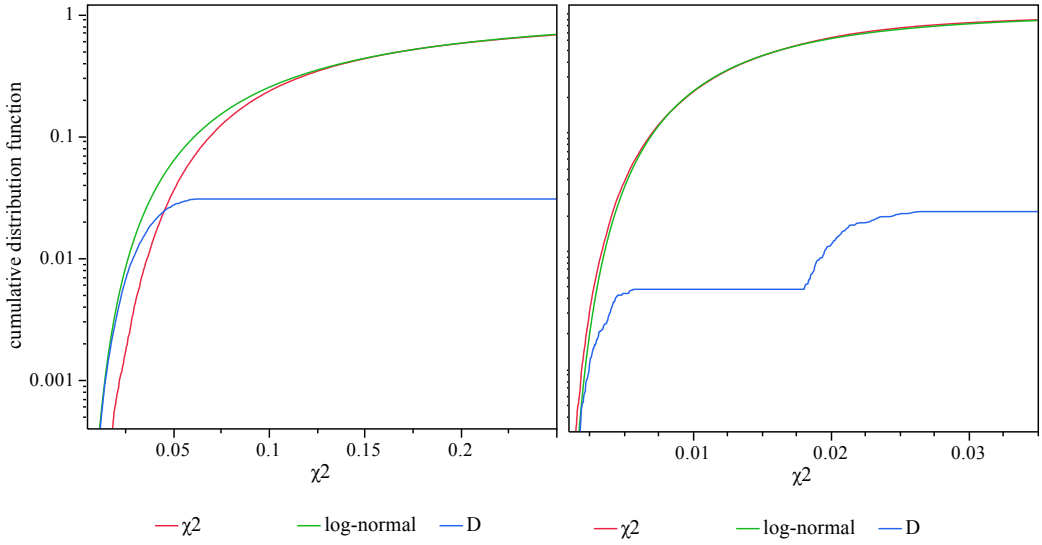

Figure 2.16 The CDF for the distribution of χ^2 of 10^5 simulated models with fifteen to nineteen modes against the fifteen normalized frequencies of BPM 37093 identified by Kanaan *et al.* (2005). The CDF for the log-normal distribution and the increasing maximum deviation between each CDF are also included.

line in the right panel of Figure 2.16 to the blue line in Figure 2.15. The scale changes but the shape stays the same as well as the value of the CDF at the lower and upper plateaus.

We compare the simulation of a goodness-of-fit test for BPM 37093 to a grid of 100 000 "stars" with randomly generated modes. By comparing the observed frequencies to a distribution of simulations similar to those seen in §2.5.5, i.e. Figure 2.12 and Figure 2.13, we may see if sets of observations perform better in these simulations than in random sets. To make the comparison, we utilize the statistics from the simulation using the normalized frequencies. When the fifteen pulsation frequencies are fitted to a group of fifteen random model modes, BPM 37093 has a mean χ^2 better than only 60% of 100 000 simulated stars and a median better than only 70%. Kolmogorov's D is lower than only 40% of the simulations and 60% of the simulations have a significance smaller than 10^{-45}. When the fifteen observed modes are fitted to a group of nineteen simulated model frequencies, BPM 37093 has a mean χ^2 better than 50% of the 100 000 "stars" and a median better than only 20%. Kolmogorov's D is better than 90% of the simulations, but Q is still very low: 4.35×10^{-40}. When comparing

the statistics of the distribution of χ^2 as opposed to finding the closest matching model, the observed pulsations of BPM 37093 do not appear to produce any results distinguishable from simulated stars.

2.7 Potential for further work

By exploring the functional form for the distribution of the quality-of-fit of a "best model" to a given set of "observed" frequencies, we find no universal form for the expected significance level. There may be an analytic way of determining the quality of fit of a model through targeted simulations and "brute force" calculation of a cumulative distribution function. These tests may require statistics previously unexamined, like the lowest χ^2 among the models or the range of modes for the star or model. We do not show many examples of testing distributions of χ^2 between sets of random modes with actual observed pulsations, but we will do so in a later chapter where we evaluate the quality of published results.

CHAPTER 3. DETECTING AND TESTING MODE SPACINGS

In tuning models by matching observed and theoretical periods, astrophysicists have a powerful tool for understanding stellar interiors. However, matching period or frequency *spacings* may provide important structural information as well with less intensive computations. Recall in §1.2 that nonradial oscillation modes with high radial order exhibit an asymptotically fixed spacing. Oscillations with an equal frequency spacing, σ_0, determined by the the inverse of the sound crossing time as shown in Equation 1.4, are classified as p-modes. Examples of these oscillations are seen in the Sun or solar-like stars. Pulsations with equally spaced periods, g-modes, are seen in white dwarfs and some pulsating subdwarf B (sdB) stars (Reed *et al.* , 2010). Researchers work with equally spaced sets of modes because they better constrain intrinsic properties of the star and identifying and modeling spacings is easier than individual frequencies.

3.1 Observed spacings

3.1.1 Frequency spacings in helioseismology

A number of ground- and space-based efforts are quite fruitful in detecting frequency spacings within the Sun using Doppler velocity measurements as review articles such as Libbrecht (1988) and Christensen-Dalsgaard (2002) offer in detail. For example, Libbrecht (1988) presents a plot, reprinted here as Figure 3.1, showing the agreement between the observed p-modes from Duvall *et al.* (1988) and the theoretical p-modes obtained from a standard solar model (Christensen-Dalsgaard *et al.* , 1985). The plot shows the frequencies, $\nu_{n\,\ell}$, of each p-mode versus degree, ℓ, and the modeled frequencies are connected by lines of fixed radial order, n, for clarity. The modes of degree $\ell = 0$, 1, 2 and 3 from Duvall *et al.* (1988) are also

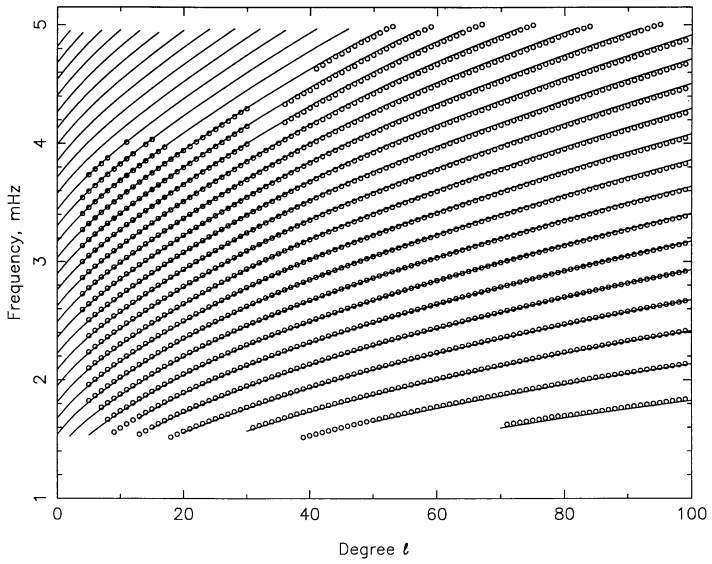

Figure 3.1 The measured p-mode frequencies of the Sun (Duvall *et al.* , 1988), $\nu_{n\,\ell}$ plotted as circles, alongside the theoretical p-mode frequencies calculated from a solar model (Christensen-Dalsgaard *et al.* , 1985). The modeled frequencies are connected by "ridge lines" of fixed n, starting with $n = 2$ in the lower right and increasing by one for each higher ridge. Reprinted from Libbrecht (1988).

plotted on an échelle diagram in Figure 3.2. The échelle diagram, previously discussed in §2.1, has a folding frequency, $\Delta\nu$, of 135μHz which corresponds to a sound travel time between the surface and the center of the Sun of about an hour, i.e. the solar dynamic time scale. Equally spaced frequencies would fall on a vertical line on the échelle diagram in keeping with the asymptotic analysis by Tassoul (1980). However, variations in structure near the solar surface (Christensen-Dalsgaard & Pérez Hernández 1992, Christensen-Dalsgaard 2003) make the spacing less uniform which induces a slight curvature in the line of frequencies. Recall in §2.1 that Guenther *et al.* (2005) uses this technique in an attempt to identify real oscillations in η Boo.

3.1.2 Period spacings in white dwarfs

White dwarfs have detectable g-mode pulsations which, for high radial order, have equal period spacing under asymptotic analysis. Two prominent examples of multi-periodic mea-

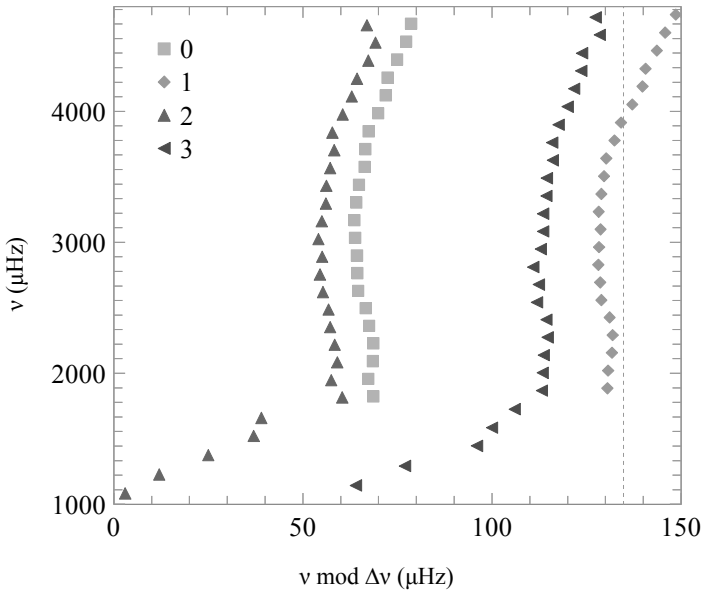

Figure 3.2 An échelle diagram for solar pulsation frequencies from Duvall *et al.* (1988) with degree ℓ =0, 1, 2 and 3. The dotted vertical line indicates the folding frequency, $\Delta\nu$.

surements of white dwarfs are the Whole Earth Telescope (WET) observing campaigns of PG 1159–035 (Winget *et al.* , 1991) and GD 358 (Winget *et al.* , 1994). While these works yield many oscillation modes, some frequencies predicted by models are not present in the power spectra. In addition to these "missing" modes, other modes with different values of ℓ found in the same star have different spacings as inferred from Equation 1.2. Having *two* spacings present complicates the pattern and makes identification of uniform period spacings problematic.

3.2 Evaluating mode spacings

3.2.1 Kolmogorov-Smirnov test

Using earlier results for PG 1159–035, Kawaler (1988) sets up an algorithm examining the quotient of the difference between a given pair of periods and a given spacing. If the period spacing is present among all the modes, all of the quotients should be integers; otherwise, the difference between the quotients and their proximate integers, called the residuals, would be

evenly distributed from 0 to 1. Kawaler (1988) uses the K–S test first discussed in §2.4 to find the significance, Q, of the distribution of residuals. A smaller value of Q means the residuals are not well distributed and there is evidence supporting a prospective period spacing. By expressing the significance of a spacing as $\log Q$, prominent spacings register as minima when plotting $\log Q$ versus $\Delta\Pi$.

An example of the test can be seen in Figure 3.3, reprinted from Winget *et al.* (1991), which displays the results of the test conducted on the oscillation periods of PG 1159 obtained from a WET observation run. The Figure presents an unanticipated result: the peaks

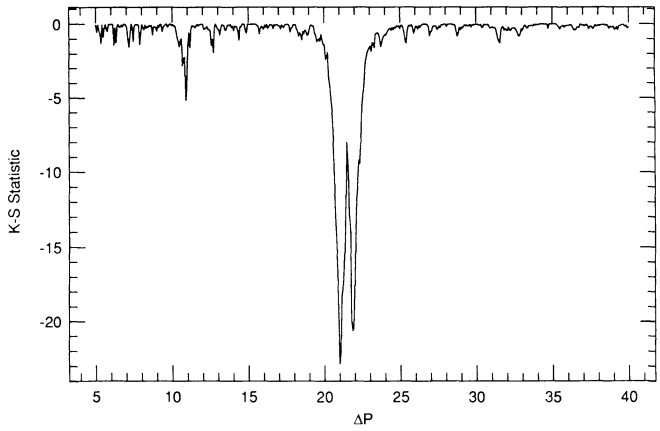

Figure 3.3 Reprinted from Winget *et al.* (1991), the K–S test for the measured pulsation periods of PG 1159–035. The best spacings are minima in $\log Q$. Note the bifurcation of the 21 s spacing.

associated with mode spacings are clearly bifurcated. Winget *et al.* (1991) account for the anomaly as an effect of mode trapping; the radial nodes associated with some of the pulsation modes may coincide with a layer boundary in the star. The asymptotic relation leading to the equal spacings assumes a homogeneous star but several models of stars e.g. white dwarfs show clear, compositionally differentiated strata with such boundaries.

We must take a few things into consideration with the K–S test. Since only the selected periods are used, the test omits a considerable amount of data present in period spectra. Choosing the period is a subjective process and the test does not account for the reported uncertainties of the modes nor their amplitudes.

3.2.2 Fourier Transform of the Period Transform

When analyzing the observed modes of PG 1159, Winget *et al.* (1991) compare the results of the K–S test to a separate technique for discerning spacings. The method converts the frequency spectrum produced from observations to a period spectrum, i.e. a period transform, and performs a Fourier transform of the period transform (FTPT). Peaks in the FTPT correspond to significant spacings. For a comparison between the tests, we reprint Figure 3.4 from Winget *et al.* (1994) where the FTPT plot for another WET target, the white dwarf GD 358, is superposed above the K–S test plot. The highest peak in the FTPT matches the minimum $\log Q$ in the K–S test for both PG 1159 and GD 358.

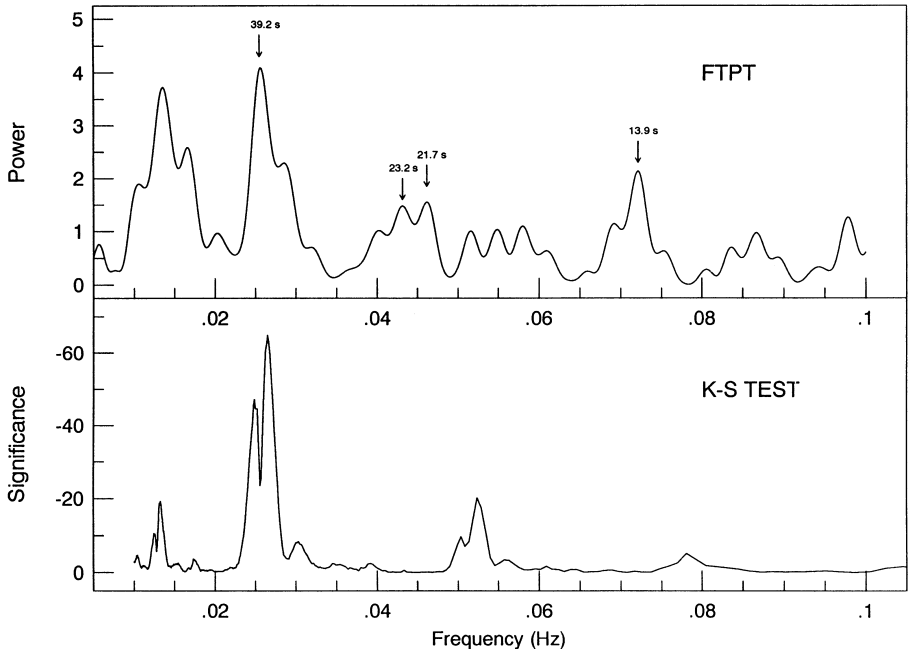

Figure 3.4 Above panel: The Fourier transform of the period transform (FTPT) for the white dwarf GD 358. Lower panel: the K–S test results with a reversed ordinate for the same star. Reprinted from Winget *et al.* (1994).

Unlike the K-S test, the FTPT is completely objective in using the whole period spectrum. However, the period transform is non-sinusoidal and the peaks contain little power overall compared to the noise. As a result, the FTPT generates harmonic peaks as well as high-period

noise peaks. Any user of the FTPT must remain vigilant in identifying and ignoring these impostors. The K-S test also produces harmonic peaks as well as low-period or low-frequency noise peaks depending on the spacing being tested, but they are at lower significances and are mitigated when aliasing is limited with time-distributed observations.

While the FTPT is only used to find period spacings in white dwarfs, a Fourier Transform of the frequency spectrum may conceivably be used to find the frequency spacings inherent in p-mode pulsations.

3.2.3 Inverse Variance Test

O'Donoghue (1994) presents an alternative method for finding spacings by comparing a set of modes with a fitted set of equally spaced values. Using the residuals between corresponding modes in each set, the technique tests a given spacing's validity by examining the inverse variance. Legitimate spacings correlate with high inverse variances.

These values are fitted to an optimal mode from the observations, e.g. the pulsation with the highest amplitude, Π_0. Using a trial spacing, $\Delta\Pi$, the fitted value, c_i, is an integer number of spacings, k_i, from our fitting mode and is as close as possible to the observed mode, Π_i. To ensure equally sized sets and to avoid a trivial variance for Π_0, O'Donoghue (1994) sets c_0 to match with Π_0,

$$c_0 = \sum_{i=1}^{N} \frac{\Pi_i - k_i\,\Delta\Pi}{N-1} \ . \tag{3.1}$$

The residuals are scaled by the size of the spacing to favor larger spacings versus any possible harmonics. While the statistical variance of a population calculates the difference between each element and the mean, the variance,

$$\sigma^2 = \frac{1}{N}\sum_{i=1}^{N}\left(\frac{\Pi_i - c_i}{\Delta\Pi}\right)^2 \ , \tag{3.2}$$

uses the scaled residuals in place of that difference, and the inverse variance would be the reciprocal of σ^2. Like the K-S test, the inverse variance test results appear much cleaner when non-spaced modes are discarded. Figure 2 of O'Donoghue (1994), reprinted as Figure 3.5, shows the inverse variance for all PG 1159 modes against the inverse variance for just the

$\ell = 1$ modes. The peak inverse variance matches the peak of the FTPT and the center of the bifurcation from the K-S test from Figure 3.4 and it does not suffer from duality.

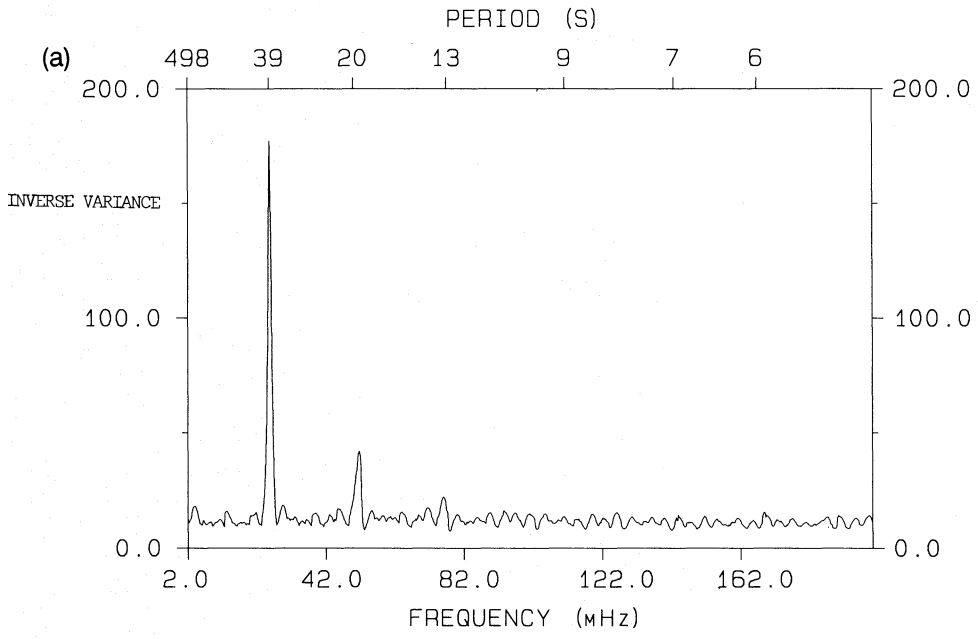

Figure 3.5 The inverse variance for the oscillation periods of the white dwarf GD 358 measured by the WET. Reprinted from O'Donoghue (1994).

3.3 Finding random period spacings with the K–S test

Although these techniques are used to process incomplete information about a given star's oscillations, those missing modes may influence the tests to make erroneous conclusions such as indicating a spacing that is merely coincidental between the identified modes. The ideal method would be able to discern a mode spacing with physical meaning from one produced by chance. By testing these techniques with sets of random numbers, we can learn how frequently the tests show evidence for spacings irrelevant to a star's intrinsic properties.

As stated in §3.2.1, Kawaler (1988) utilizes the Q parameter to find the optimal spacing in frequency or period for the modes observed in a pulsating star. While the value of $\log Q$ can show the significance of a particular mode spacing, the parameter is not applied yet to a multitude of models composed of random modes in a manner similar to the procedure we

conduct in §2.3. With this in place, we may quantify the statistical significance of an identified spacing yielding a given value of Q.

We use ran2 from Press *et al.* (1992) once again, producing 10^6 sets of random modes over a normalized range. The algorithm devised by Kawaler (1988) determines the lowest value of Q for each set as well as the spacing corresponding to that minimum. The results present $\log Q$ to showcase the minimum values of Q. This would provide a basis of comparison for prospective mode spacings. With the range of significances set as benchmarks, the significance of an observed spacing, i.e. the value of Q, can translate into a confidence measure by comparing it with the spacings found in a random selection. For a point of comparison, Kawaler (1988) finds a strong minimum in $\log Q$ for a period spacing in the 8 modes identified in PG 1159 by Winget *et al.* (1985). These findings are later supported by Winget *et al.* (1991). We shall discuss if it is truly a significant spacing in §4.1 and if Kawaler (1988) has some good fortune by making the correct claim with the data available at the time.

3.4 Removal of ill-fitting modes for a determined spacing

Some of the modes observed in a star do not share the same spherical harmonic indices as the other pulsations and do not adhere to the associated spacings. The program is configured to detect which modes fit the spacings better than others. With this in place, the program eliminates the interloping modes from the set to improve its significance or its standing among random models.

The inverse variance technique presented by O'Donoghue (1994) includes a method that would serve this purpose. Given a set of observed modes, a_i, $i = 1 \ldots N$, we construct a set consisting of modes close to the observed values but spaced by the best spacing evaluated for the star, Δa. Each element in the fitted set, c_i, $i = 1 \ldots N$, is configured using its corresponding observed mode, a_i, as well as a "centering" mode, a_0, left to a user's discretion. The centering mode can introduce some bias into the technique especially if the optimal spacing does not match well with that mode. The fitted element, c_i, differs from the centering mode by an

integer multiple of Δa, setting it as close as possible to a_i. The integer is denoted by k_i,

$$c_i = a_0 + k_i \, \Delta a \ . \tag{3.3}$$

If some of the observed modes are close enough, e.g. a multiplet, their fitted modes would likely have the same value. While we would likely want to keep the centering mode in the trimmed set, Equation 3.3 would lead to at least one c_i having the same value as a_0. O'Donoghue (1994) accounts for this by using the other elements of a_i and c_i to construct c_0,

$$c_0 = \sum_{i=1}^{N} \frac{a_i - k_i \, \Delta a}{N - 1} \ . \tag{3.4}$$

The discrepancy between N terms in the summation and $N - 1$ in the denominator is because the term containing a_0 is trivial. After removing the observed mode with the greatest deviation from its fitted value, the program recalculates the significance of the remaining set. Following that, the user has the option to repeat the removal-and-recalculation procedure.

The mode-removal algorithm has some general results. If one mode noticeably deviates from the chosen spacing, removing it would make the set less uniformly distributed. This increases D and has a greater effect on Q than the slight decrease in N. However, the algorithm can increase the value of Q, i.e. decreasing the significance of the period spacing, if every mode is closely matched to a fit or there were few mode differences at the outset.

3.5 Results of the simulations

The main outcome of these simulations is a percentile assignment to the Q value for a given spacing analysis. The percentile for a given Q from the K–S test refers to the fraction of simulations that produce a Q value that is less significant. For example, if an observed spacing has a Q value that has a percentile rank of 99%, only 1 in 100 random trials produce a better value. The results of these simulations are shown in Figure 3.6 through Figure 3.15. Each set of data is displayed in four separate Figures; e.g. the distribution of the lowest values of Q for 10^6 simulated stars with eight modes is shown in the two images in Figure 3.6 and the two images in Figure 3.7. Since the images in Figure 3.6, Figure 3.8, etc. use a linear scale for the $\log Q$ axis, as opposed to the logarithmic scale used in Figure 3.7, Figure 3.9, etc., we shall refer

to the former Figures as the linear Figures and the latter Figures as the logarithmic Figures. The simulated stars used to generate the five curves in each Figure have one fundamental difference: they do not begin with the same number of modes at the onset. After the initial evaluation of the optimal spacing, up to four modes are removed by the procedure explained in § 3.4. For example, the orange curve labeled "3" in Figure 3.6 initially contains eleven modes.

To better interpret the data, we sort the myriad $\log Q$ minima and determine the percentile of the distribution at certain points. We initially find the elements of the set at the 50^{th}, the 90^{th}, the 99^{th}, the 99.9^{th} and the 99.99^{th} percentiles. Unfortunately, this leaves us with a limited number of values to examine and thoroughly compare the effects of removing an "extra" mode. These "benchmarks" are shown in Table 3.1 through Table 3.5. We choose instead to separate the best Q values into bins segmented by integer values of $\log Q$. The size of each bin allows us to determine the percentile at each division, which provides the data points seen in each Figure.

Table 3.1 Percentile for 8 modes to generate a certain Q parameter with $M - N$ extra modes removed. Test performed for 10^6 simulated stars.

Percentile	**0**	**1**	**2**	**3**	**4**
50.00%	−4.02	−5.12	−5.35	−5.53	−5.70
90.00%	−6.13	−8.04	−8.79	−9.23	−9.61
99.00%	−8.87	−11.23	−12.32	−13.05	−13.61
99.90%	−11.44	−13.98	−15.06	−15.87	−16.53
99.99%	−13.70	−16.31	−17.41	−18.14	−18.60

Table 3.2 Percentile for 9 modes to generate a certain Q parameter with $M - N$ extra modes removed. Test performed for 10^6 simulated stars.

Percentile	**0**	**1**	**2**	**3**	**4**
50.00%	−4.00	−5.14	−5.44	−5.66	−5.88
90.00%	−6.20	−8.19	−9.11	−9.74	−10.24
99.00%	−9.12	−11.71	−13.02	−13.96	−14.72
99.90%	−11.98	−14.89	−16.29	−17.29	−18.05
99.99%	−15.00	−17.87	−19.16	−20.02	−20.71

The first images in the linear Figures each show nearly the entire range of the best values of

Table 3.3 Percentile for 10 modes to generate a certain Q parameter with $M - N$ extra modes removed. Test performed for 10^6 simulated stars.

Percentile	**0**	**1**	**2**	**3**	**4**
50.00%	−3.98	−5.13	−5.49	−5.77	−6.02
90.00%	−6.27	−8.26	−9.36	−10.16	−10.79
99.00%	−9.35	−12.02	−13.54	−14.72	−15.65
99.90%	−12.53	−15.61	−17.24	−18.41	−19.54
99.99%	−15.59	−18.87	−20.36	−21.55	−22.58

Table 3.4 Percentile for 11 modes to generate a certain Q parameter with $M - N$ extra modes removed. Test performed for 10^6 simulated stars.

Percentile	**0**	**1**	**2**	**3**	**4**
50.00%	-3.98	−5.11	−5.53	−5.85	−6.13
90.00%	-6.32	−8.30	−9.53	−10.47	−11.24
99.00%	-9.54	−12.30	−13.94	−15.33	−16.45
99.90%	-12.90	−16.06	−17.94	−19.46	−20.74
99.99%	-16.52	−19.83	−21.59	−23.23	−24.23

Q, and the percentiles in each curve reach a plateau around −14 and appear to be populated by extreme outliers beyond that point, i.e. well-spaced values. All of the curves in each Figure follow some general trends. Looking at the red curves where no modes are removed, there is a sharp increase in percentile between −2 and −6 and the curves reach the plateau around −9. By comparison, the other curves have a more gradual slope which implies that the distributions are greatly shifted to lower values of Q. However, removing additional modes result in less appreciable change as evidenced by the tighter grouping between the other curves compared

Table 3.5 Percentile for 12 modes to generate a certain Q parameter with $M - N$ extra modes removed. Test performed for 10^6 simulated stars.

Percentile	**0**	**1**	**2**	**3**	**4**
50.00%	−3.98	−5.09	−5.55	−5.90	−6.21
90.00%	−6.38	−8.32	−9.63	−10.70	−11.59
99.00%	−9.73	−12.44	−14.28	−15.79	−17.10
99.90%	−13.35	−16.55	−18.58	−20.30	−21.72
99.99%	−16.93	−20.65	−22.61	−24.38	−25.78

to the red curve.

To better illustrate these minor differences, we present the second image in the linear Figures which only conveys the region where the slopes of the curves taper off. The top 20% of each curve is displayed more prominently in these images, which gives a rough idea of the threshold for spacings that could be considered "real" and not easily reproduced.

While the latter images magnify the differences between the curves at, for example, a $\log Q$ of -10 in Figure 3.6, we find some use in showing the curves on a logarithmic plot. These plots are shown in Figure 3.7, Figure 3.9, etc., and shall be referred to as the logarithmic Figures. These Figures plot the percentiles as "the top 1%" instead of "the 99^{th} percentile" in order to better discern the plateaus of each curve, i.e. the distribution of the outlying values of $\log Q$. As we see in the median region of the distribution, the curves resulting from filtered modes are bunched together away from the red curve. In several of the Figures, the red curve approaches the end of the distribution and hits a logarithmic plateau since the best element in a distribution of 10^6 values would be "the top 0.0001%." The second images in the logarithmic Figures have a range from the 80^{th} percentile to the 99.91^{st} percentile which is intended to display roughly the same region as is shown in the second images of the linear Figures. Since the top 10% is our greatest concern in these distributions, this image provides greater focus to the threshold region mentioned earlier.

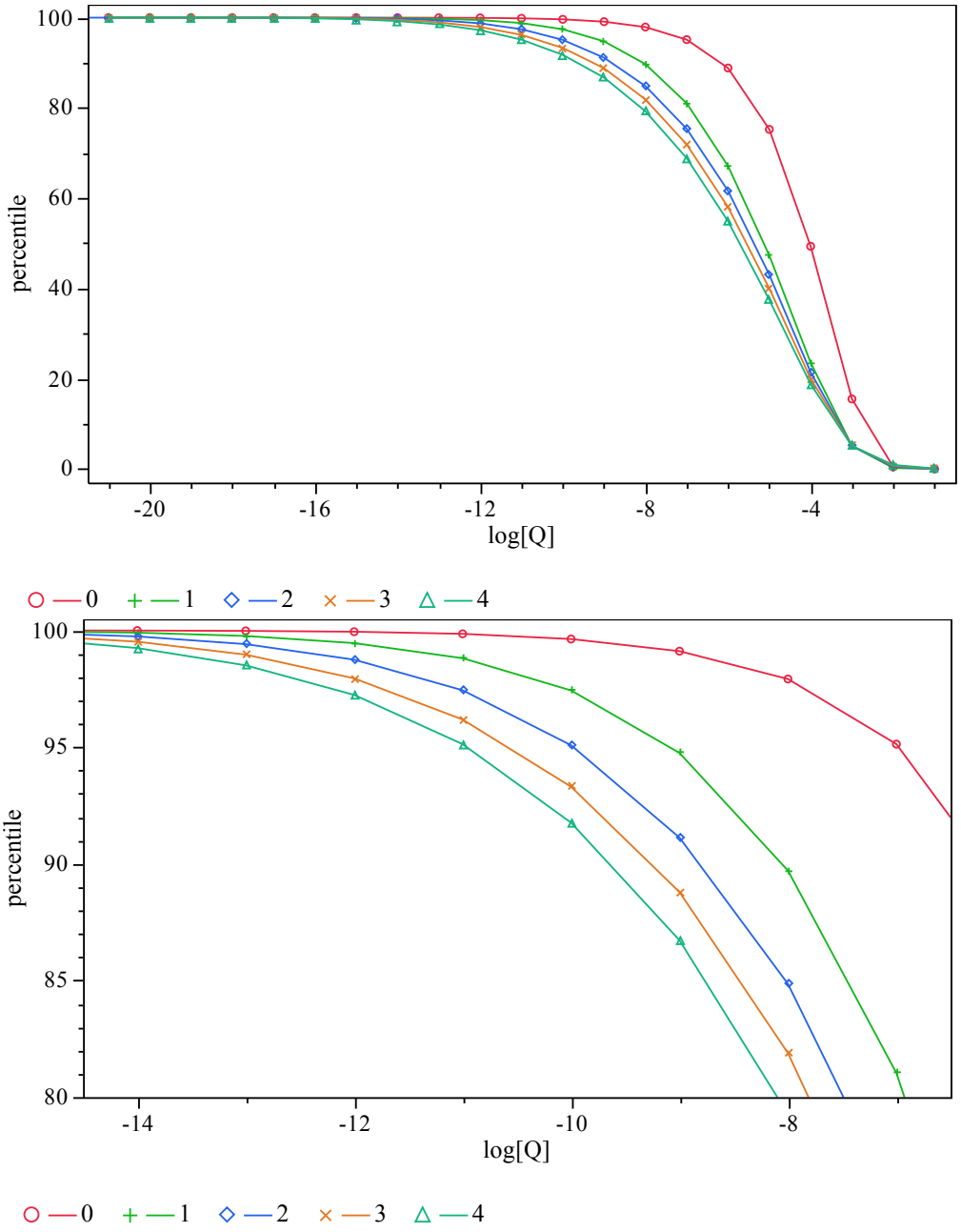

Figure 3.6 Red: The distribution of the best Q found for 10^6 simulated stars with eight modes. The other curves show the distribution of Q when a number of modes (up to four) are filtered out from the original set.

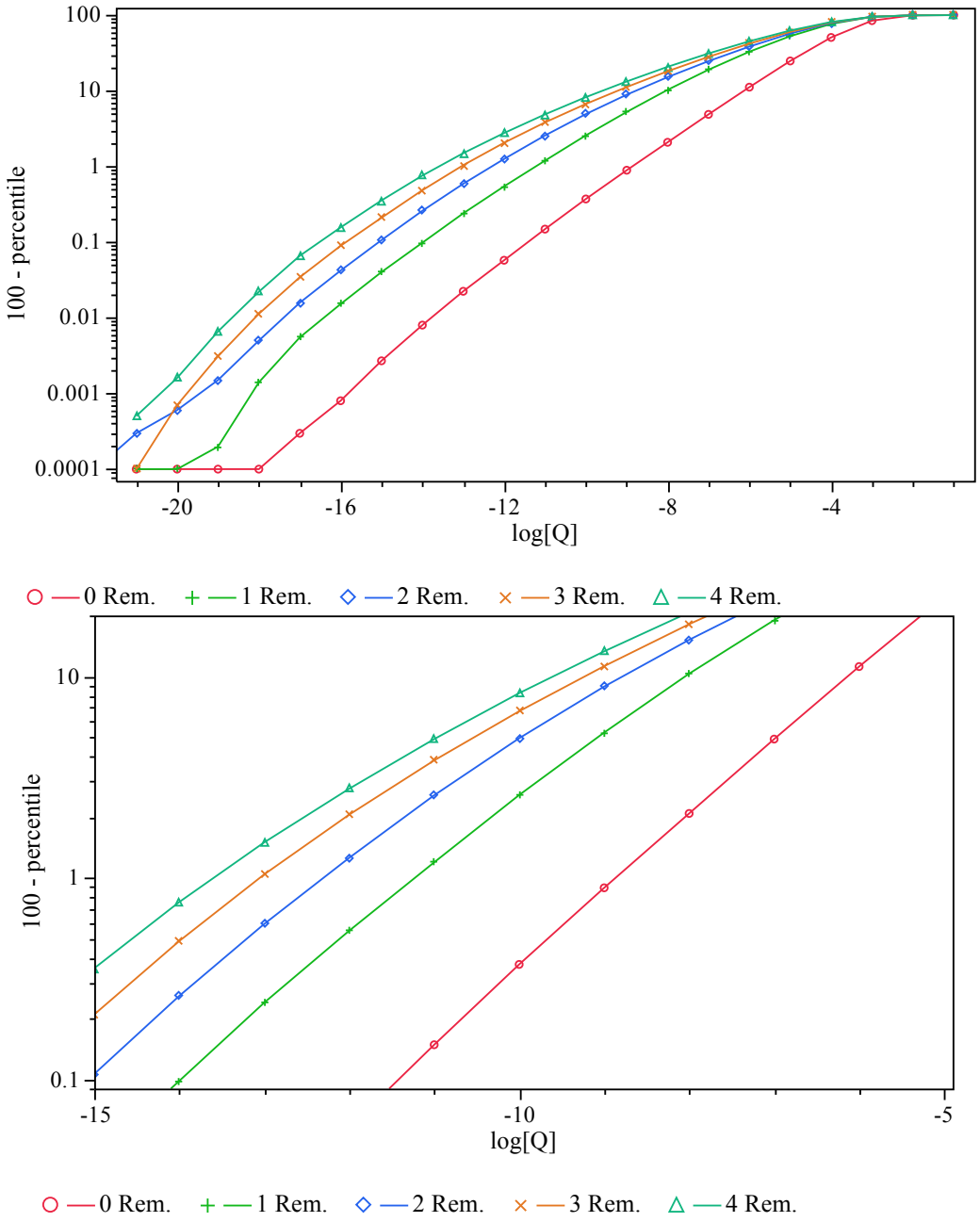

Figure 3.7 Red: The distribution of the best Q found for 10^6 simulated stars with eight modes. The other curves show the distribution of Q when a number of modes (up to four) are filtered out from the original set.

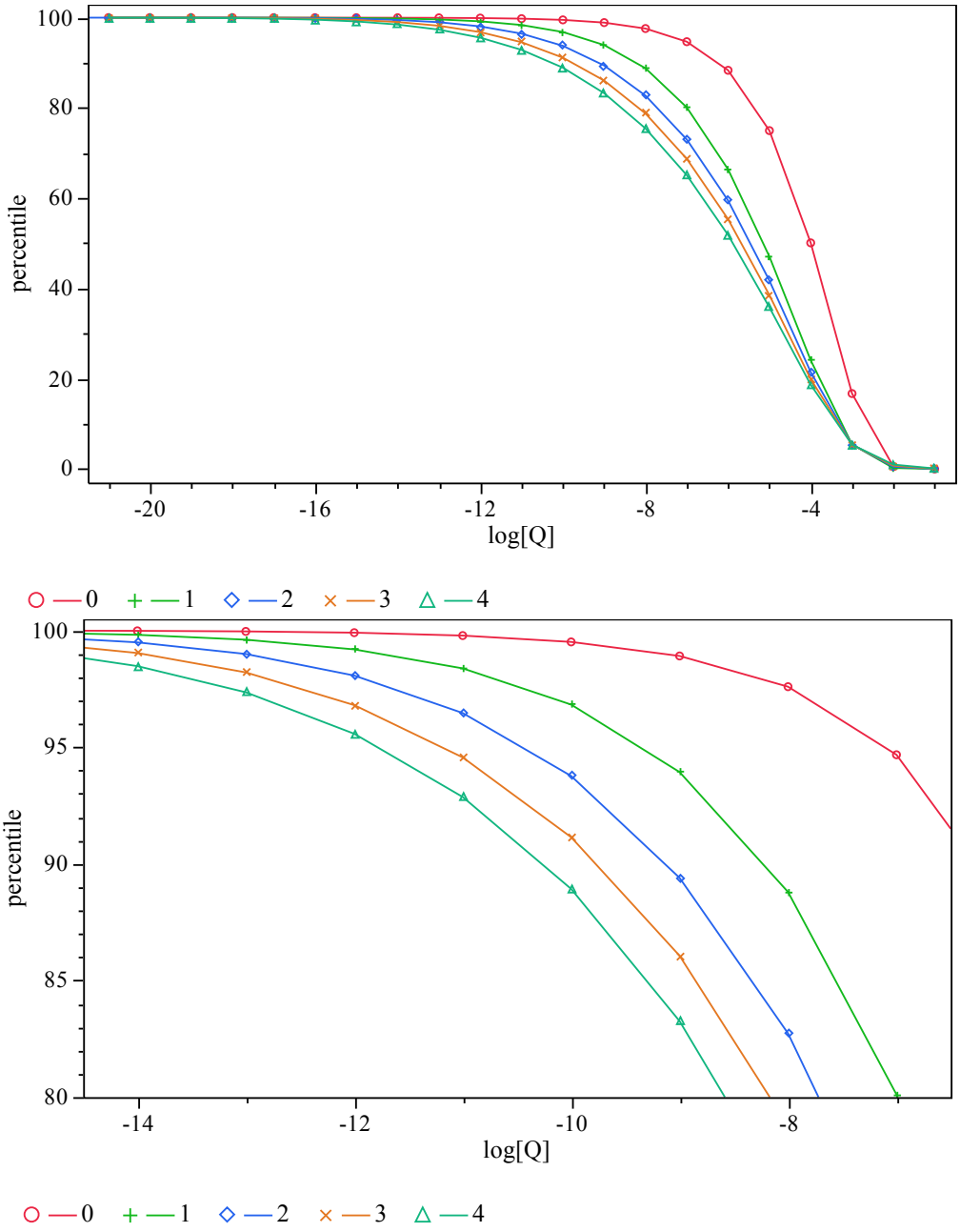

Figure 3.8 Red: The distribution of the best Q found for 10^6 simulated stars with nine modes. The other curves show the distribution of Q when a number of modes (up to four) are filtered out from the original set.

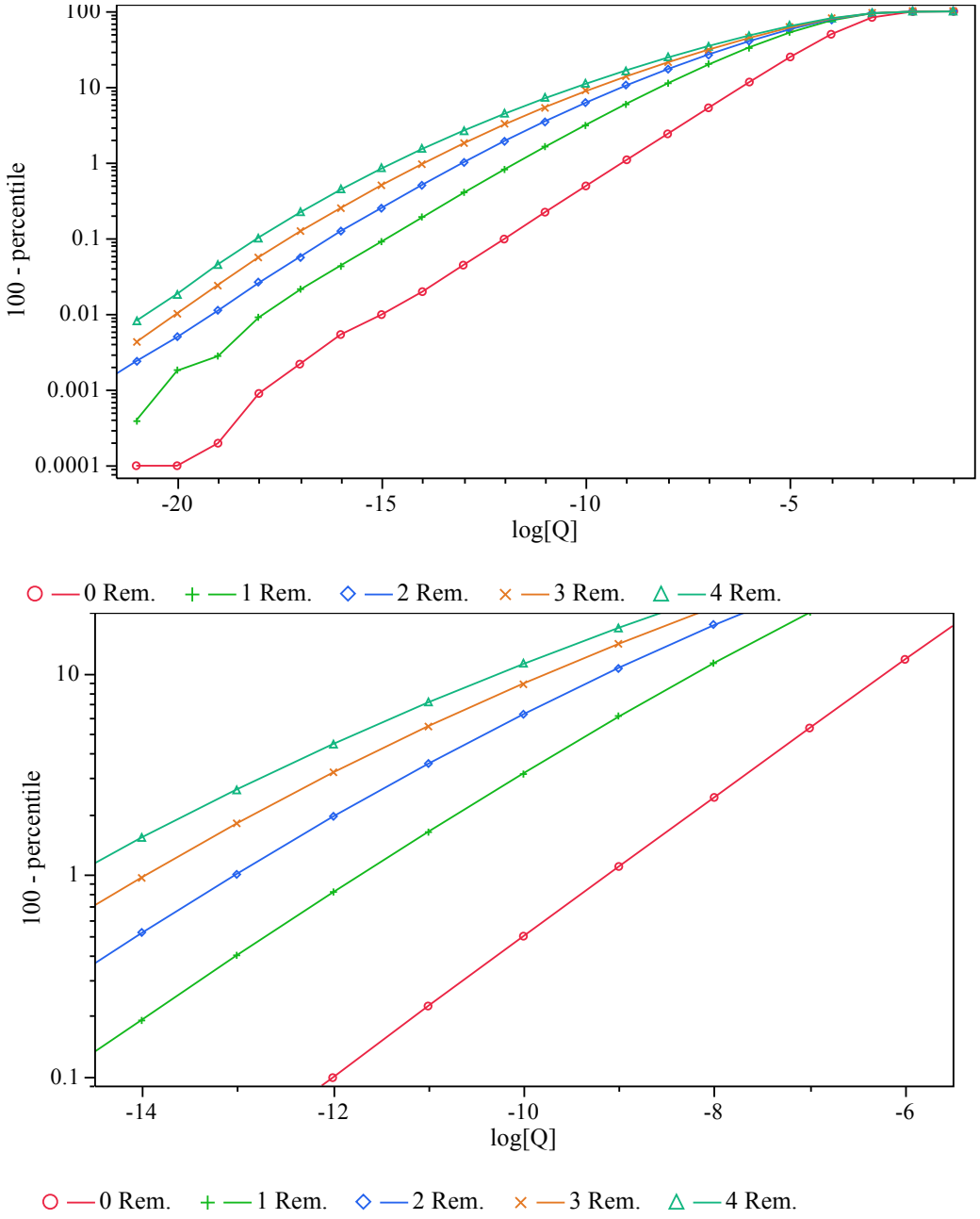

Figure 3.9 Red: The distribution of the best Q found for 10^6 simulated stars with nine modes. The other curves show the distribution of Q when a number of modes (up to four) are filtered out from the original set.

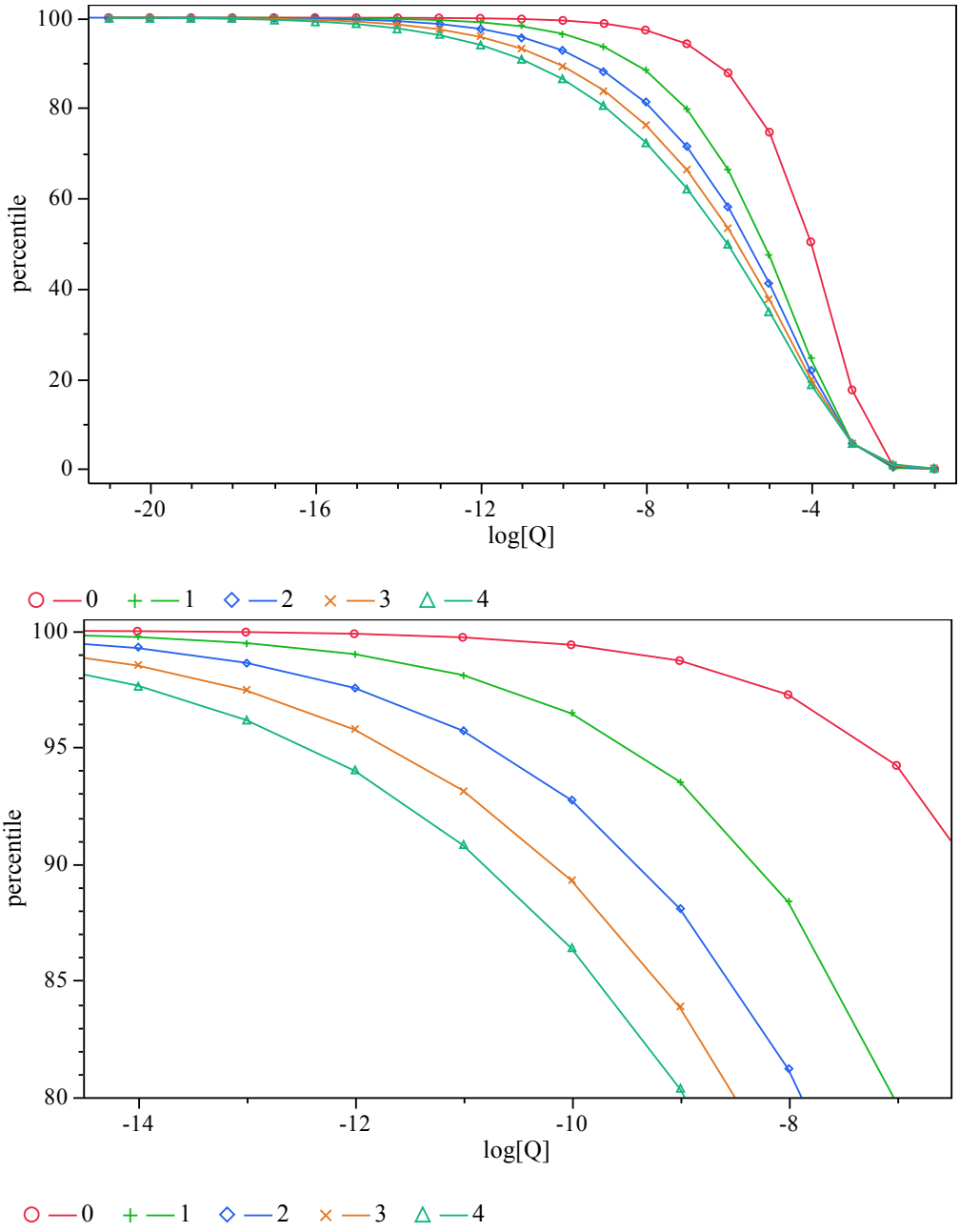

Figure 3.10 Red: The distribution of the best Q found for 10^6 simulated stars with ten modes. The other curves show the distribution of Q when a number of modes (up to four) are filtered out from the original set.

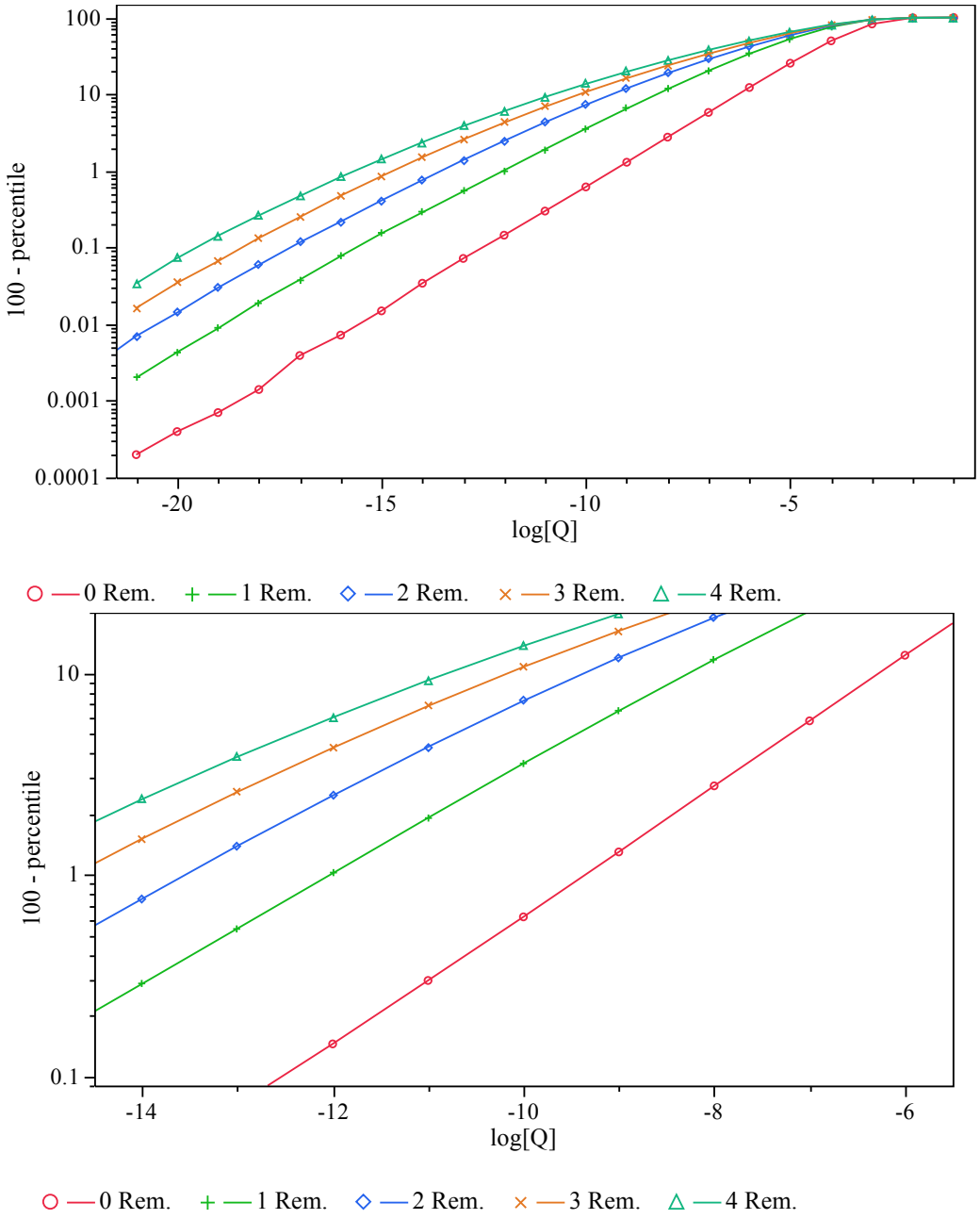

Figure 3.11 Red: The distribution of the best Q found for 10^6 simulated stars with ten modes. The other curves show the distribution of Q when a number of modes (up to four) are filtered out from the original set.

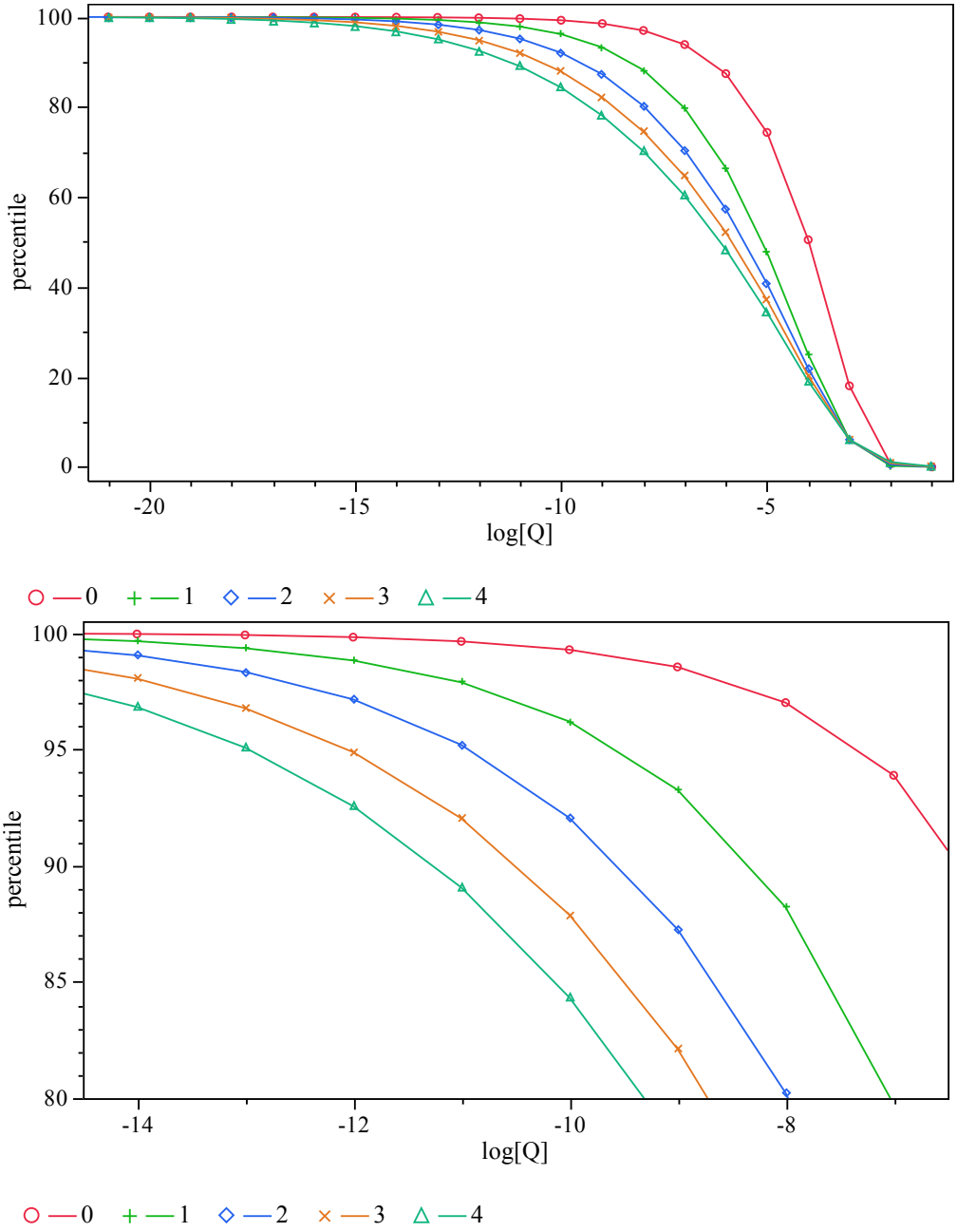

Figure 3.12 Red: The distribution of the best Q found for 10^6 simulated stars with eleven modes. The other curves show the distribution of Q when a number of modes (up to four) are filtered out from the original set.

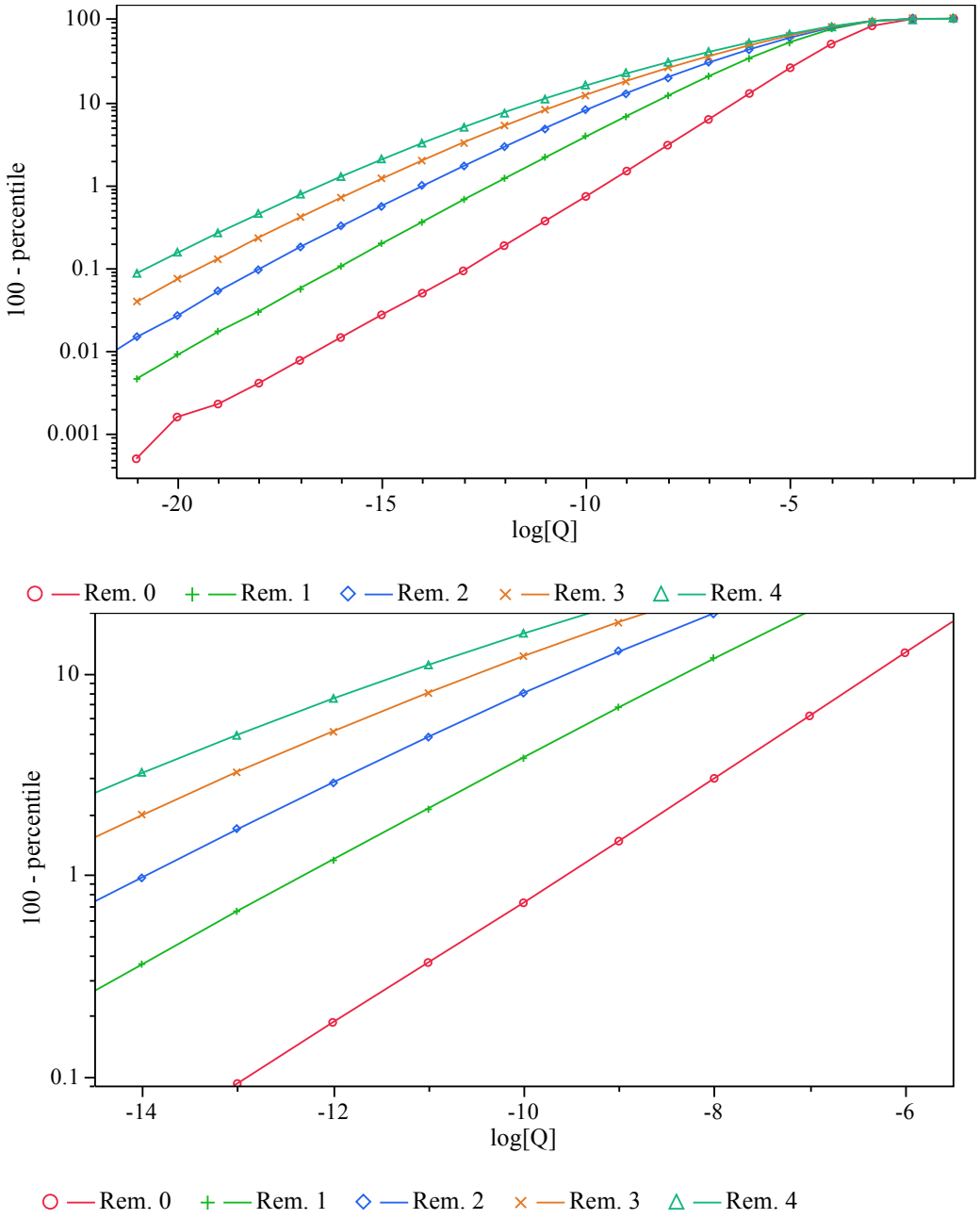

Figure 3.13 Red: The distribution of the best Q found for 10^6 simulated stars with eleven modes. The other curves show the distribution of Q when a number of modes (up to four) are filtered out from the original set.

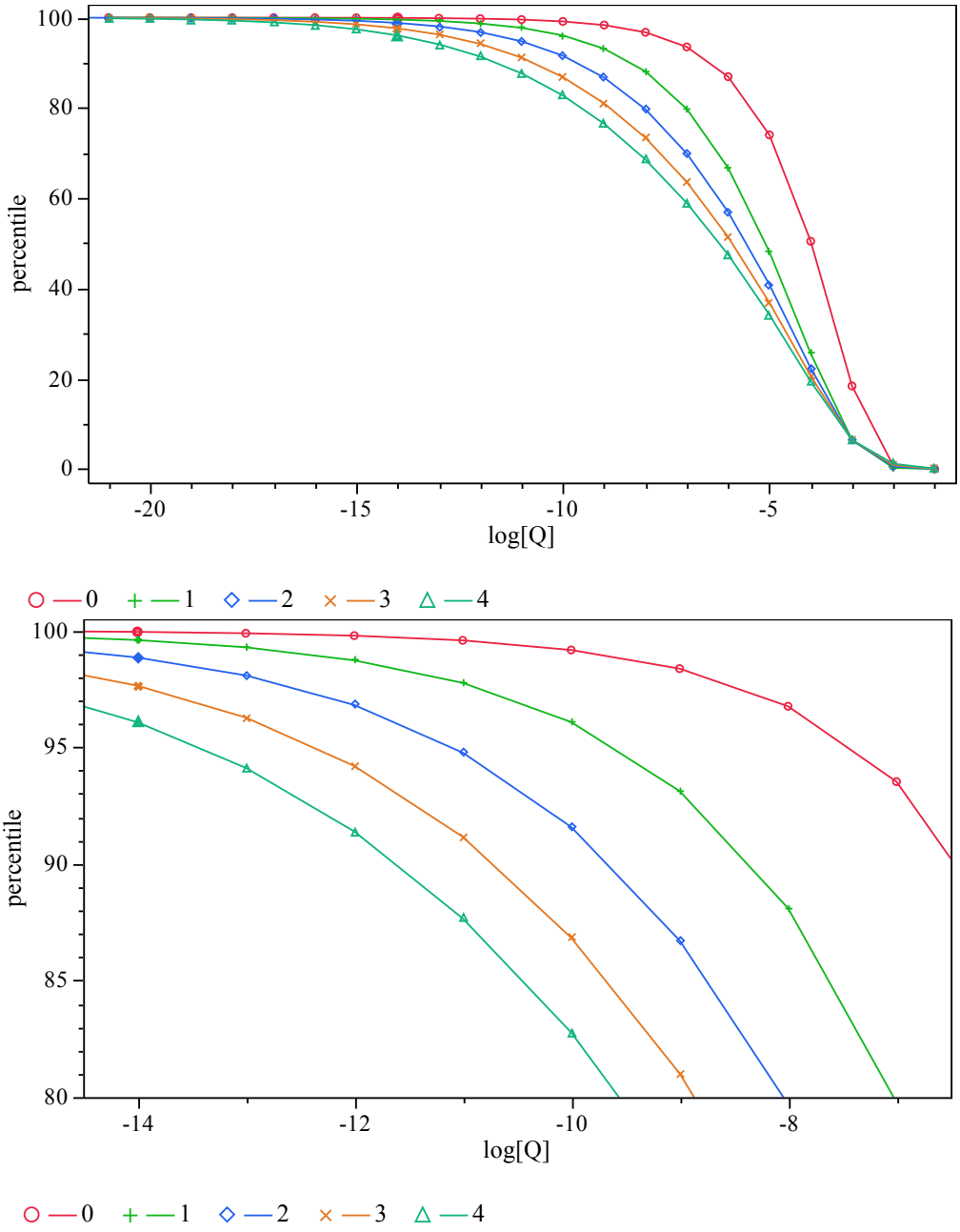

Figure 3.14 Red: The distribution of the best Q found for 10^6 simulated stars with twelve modes. The other curves show the distribution of Q when a number of modes (up to four) are filtered out from the original set.

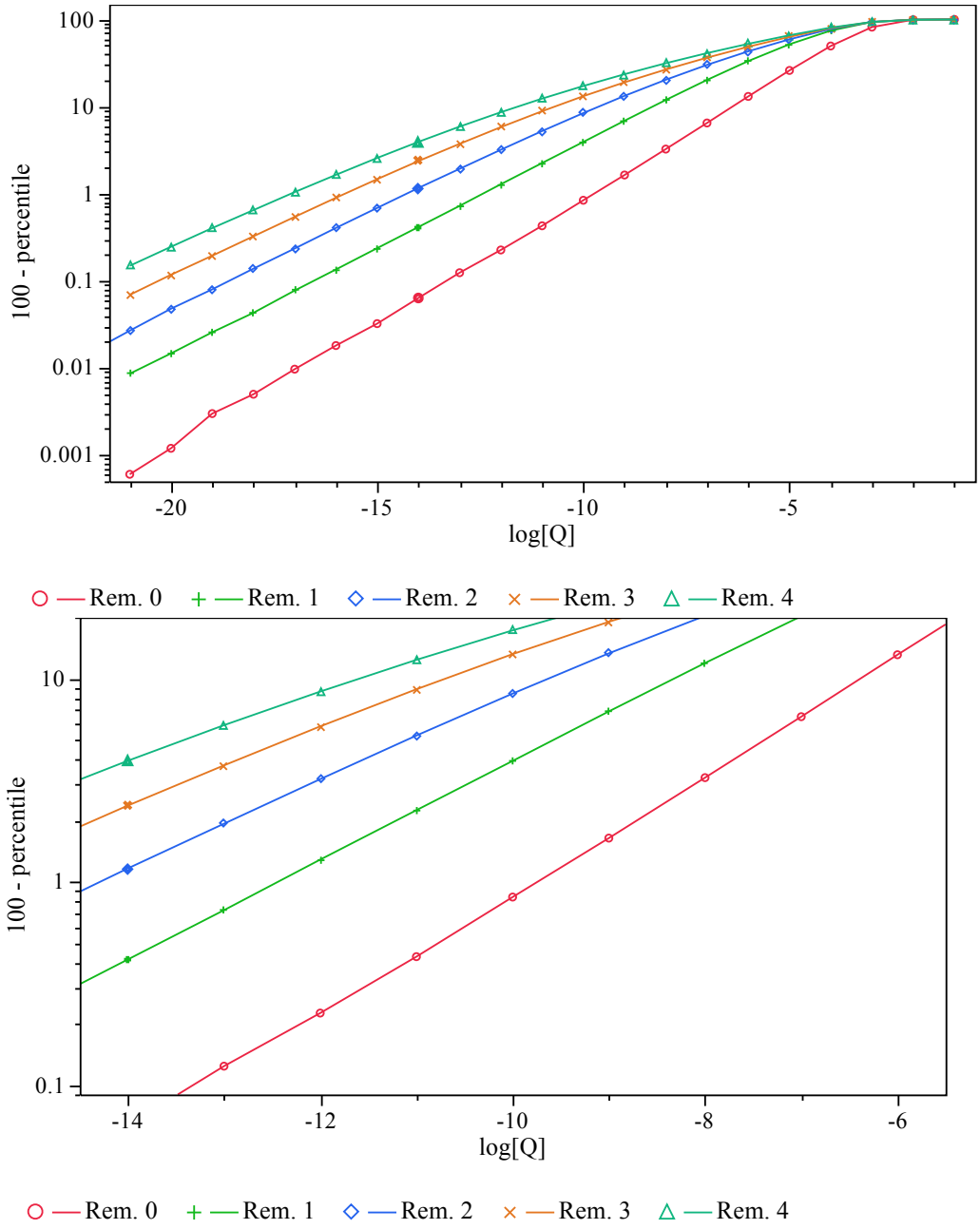

Figure 3.15 Red: The distribution of the best Q found for 10^6 simulated stars with twelve modes. The other curves show the distribution of Q when a number of modes (up to four) are filtered out from the original set.

CHAPTER 4. APPLICATION TO PUBLISHED ASTEROSEISMIC FITS

Using the simulations set up in §2 and §3, we may now review published asteroseismic studies which employ asymptotic spacings between pulsation modes. With a framework in place to judge the spacings of several stars with known pulsation patterns, we proceed to take data from the literature. For each set of data, we calculate the best spacings and their significance before and after the removal of up to four modes. However, to compare this to the curves shown in § 3.5, the data sets must contain between eight and twelve modes if none are subtracted or between twelve and sixteen modes when four are eliminated. We note each result when the comparison curve is not provided in § 3.5.

4.1 PG 1159–035

Since our work follows the general scheme outlined in prior analysis of PG 1159 (Kawaler , 1988), we prudently begin with this white dwarf. Based on reported observations of eight g-mode pulsations by Winget *et al.* (1985), Kawaler (1988) discusses two candidate period spacings for this star: 8.82 s and 21.1 s. The results for the K–S test for PG 1159 from that publication are reprinted in Figure 4.1 and they show that while the 8.8 s minimum has a lower value of $\log Q$, the 21 s minimum is wider. Kawaler (1988) compares these spacings to existing models of PG 1159 and finds the 21 s spacing corresponded to $\ell = 1$ modes while the 8.8 s would indicate $\ell = 3$ pulsations. Kawaler (1988) focuses on the larger spacing, since $\ell = 1$ modes are more likely, and later observations (Winget *et al.* , 1991) support this argument. Compare Figure 4.1 to Figure 3.3 to see the 21 s spacing become more significant with improved observations.

Our work initially focuses on the spacing with the lowest value of $\log Q$. With all eight

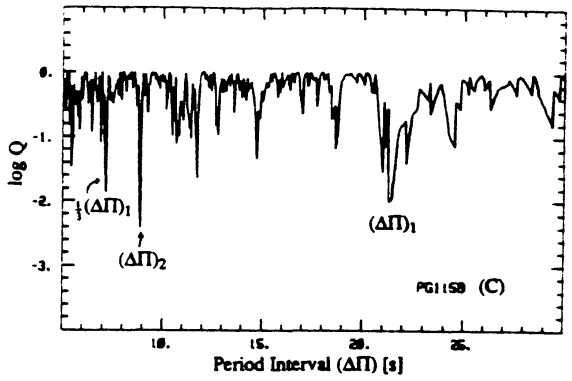

Figure 4.1 Reprinted from Kawaler (1988), the K–S test for the pulsation periods of PG 1159–035 published in Winget *et al.* (1985).

modes, the best spacing is 8.86 seconds. Table 4.1 displays the the best spacing, its significance and how it compares to random results. With $\log Q$ at -5.17, this places the set between the 75^{th} and 88^{th} percentiles, which means that a better spacing is randomly reproduced 120 000–250 000 times out of one million.

Table 4.1 also presents the results when up to four periods are removed from the set, chosen by pre-selecting a centering period as explained in § 3.4. The remaining set consists of four to seven modes whose simulations are not found on the curves in § 3.5. To show the effects of pre-selection, we test each mode as a centering mode. Since the best results with seven modes are the same for seven of the centering periods, we see that the 516 s mode does not match well with the others to this spacing which agrees with the analysis made by Kawaler (1988). When the fifth mode is omitted, the spacing becomes significantly less random. Being in the top four percent still means that up to 39 000 better spacings are reproduced out of one million.

Kawaler (1988) notes that the 424.4 s mode does not fit the 21 s spacing well and remarks that the significance of the 21 s spacing increases when that mode is removed from the set. We follow suit for our next tests with this set of modes to judge the significance of the 21 s spacing versus random sets. Table 4.2 shows the value of $\log Q$ of the $\sim$21 s spacing with eight modes as well as with the seven remaining modes which have no applicable centering mode. Since one mode is removed to produce this set of seven, we compare the results to random sets of

Table 4.1 Comparing the Q statistic of the K–S test for the eight pulsation periods of PG 1159–035 as shown in Kawaler (1988) with 10^6 sets of random numbers; spacings tested from 5–50 s; 0–4 modes removed based on centering period.

–	**best**	**log Q**	**percentile**	**center**
0	8.86	−5.17	75.2–88.8	N/A
1	8.88	−9.18	96.1–98.3	all but 516.0
2	8.87	−7.38	85.4–90.0	390.0, 451.5
3	8.86	−5.91	63.2–82.9	390.0, 451.5
4	8.83	−3.81	50.0–65.9	390.0, 451.5
2	8.88	−8.12	92.8–97.0	424.4
3	8.87	−5.94	63.2–82.9	424.4
4	8.86	−3.98	50.0–65.9	424.4
2	8.88	−8.12	92.8–97.0	495.0, 538.9, 645.2, 831.7
3	8.87	−6.48	82.9–90.0	495.0, 538.9, 645.2, 831.7
4	8.87	−3.77	50.0–65.9	495.0
4	8.86	−4.09	65.9–90.0	538.9
4	8.86	−4.12	65.9–90.0	645.2
4	8.84	−4.47	90.0–99.0	831.7
1	8.88	−3.94	11.2–32.2	516.0
2	7.18	−3.63	13.2–33.9	516.0
3	7.09	−2.56	2.39–14.2	516.0
4	9.17	−2.30	3.34–20.2	516.0

seven modes chosen from eight. This reasoning follows as more modes are removed, e.g. the row with two modes removed means that one additional mode was removed after the 424 s mode, so six periods remain in the set to compare with sets of six random modes. While the significance of the 21 s spacing increases with the exclusion of the 424 s mode, the remaining set only lies between the 54^{th} and 71^{st} percentile. With such mediocre results, Kawaler (1988) appears rather lucky in retrospect.

While the tests on the reported data from Winget *et al.* (1985) are not promising, the advent of the Whole Earth Telescope (WET) consortium brings about a vast improvement in observational capabilities. Seen in Table 4.3, the results on the data from Winget *et al.* (1991) reflect those advancements. The 21 s spacing mentioned previously takes prominence when looking at all modes or after manually paring the set down to $\ell = 1$, $m = 0$ modes. The non-spacing modes are overwhelmed by the well-spaced multiplets and the best spacing is

Table 4.2 Comparing the Q statistic of the K–S test for the 21 s spacing between the eight pulsation periods of PG 1159–035 as shown in Kawaler (1988) with 10^6 sets of random numbers; spacings tested from 5–50 s; 2–4 modes removed based on centering period, with the 424 s mode removed first.

–	**∼21 s**	**log Q**	**percentile**	**center**
0	20.94	−3.33	15.5–49.3	N/A
1	20.94	−5.77	54.1–71.6	N/A
2	20.91	−5.74	55.9–73.6	390.0, 451.5, 495.0, 516.0
3	21.13	−5.38	63.2–82.9	390.0, 451.5, 495.0, 516.0
4	21.55	−3.45	20.2–50.0	390.0, 451.5
4	21.05	−4.77	99.0–99.9	495.0, 516.0
2	20.91	−5.37	55.9–73.6	538.9, 645.2, 831.7
3	20.72	−3.35	14.2–37.9	538.9, 645.2
4	18.66	−2.20	3.34–20.2	538.9, 645.2
3	20.91	−4.88	50.0–63.2	831.7
4	22.56	−4.14	65.9–90.0	831.7

very difficult to reproduce randomly. We also test the spacing of the $\ell = 2$ modes by manually removing the $\ell = 1$ modes. The strength of the $\ell = 2$ mode spacing is also hard to match but not impossible. Promisingly, the $\ell = 1$ and $\ell = 2$ spacings are separated by a factor of $\sqrt{3}$, aligning with the expected asymptotic relationships for those spherical harmonic values as described in Equation 1.3 in §1.2.

Table 4.3 Comparing the Q statistic of the K–S test for the pulsation periods of PG 1159–035 presented in Winget *et al.* (1991) with 10^6 sets of random numbers; spacings tested from 5–50 s; varying modes removed based on centering period.

#	–	**best**	**log Q**	**percentile**	**notes**
125	0	21.04	≤ -45	≥99.9998	all
81	0	21.4	≤ -45	100	ℓ=1 or (1)
60	0	21.5	≤ -45	100	ℓ=1
20	0	21.87	−44.85	100	ℓ=1, m=0
67	0	12.32	−20.40	99.94–99.96	ℓ=2 or (2)
60	0	12.35	−23.87	99.99	ℓ=2
9	0	12.68	−12.06	99.90–99.96	ℓ=2, m=0

As expected, the significance worsens as fewer modes remain in the set; the value of Q im-

proves with additional well-spaced mode residuals and the number of residuals is proportional to N^2. While the multiplets boost the results for PG 1159, the $\ell = 1$, $m = 0$ modes still have a very strong result, bolstering our confidence in claiming that the 21 s spacing is a real spacing caused by high-overtone g-mode pulsation.

4.2 GD 358

We take data for the white dwarf GD 358 from a number of sources. The first of these is the 1990 WET run reported in Winget *et al.* (1994) and later reanalyzed by Kepler *et al.* (2003). Kepler *et al.* (2003) identify 29 pulsation periods, including a number of triplets. Table 4.4 shows these results in comparison to the 1994 WET observation campaign initially published by Vuille *et al.* (2000) and also reprinted in Kepler *et al.* (2003). The 1994 run yields 26 modes, although these modes are the same 11 multiplets as identified from the 1990 observations.

Both of the runs have very strong spacings but the multiplets appear to support a slightly shorter spacing than the $m = 0$ modes. The $m = 0$ tests fare well against random sets, but not as well as the modes found in PG 1159. When removing modes, we select different centering modes between the campaigns, preferring to use the modes with the highest amplitude instead. The tests performed on the 1994 set seem to improve with fewer modes but the 1990 set is inconclusive. Removing modes from either set results in fluctuations in the optimal spacing for the $m = 0$ modes and worsens their results. As discussed in § 3.4, if all the modes are evenly spaced, removing one or more decreases the significance.

Table 4.5 contains the results of later WET runs: the 2000 campaign detailed in Kepler *et al.* (2003), and the 2006 observations shown in Provencal *et al.* (2009). The 2006 modes have no differentiated m values so there is no test of the $m = 0$ modes. These sets follow the trends seen in the previous decade's observations: 25 or more modes have a strong period spacing at ∼38 s, although these Q values are matched by a couple random sets. The $m = 0$ modes (14 periods) from 2000 are spaced higher than previous campaigns with similar significance, but the spacing shifts less with each trimmed mode.

Table 4.4 Comparing the Q statistic of the K–S test for the pulsation periods of GD 358 from 1990s WET runs reanalyzed by Kepler *et al.* (2003) with 10^6 sets of random numbers; period spacings tested from 5–50 s; 0–4 modes removed based on centering mode.

WET campaign	**#**	**−**	**center**	**best**	**log Q**	**percentile**	**notes**
1990	29	0	N/A	37.6	≤ -45	100	ℓ=1
1990	29	1	700.6	37.7	≤ -45	100	ℓ=1
1990	29	2	700.6	37.7	≤ -45	100	ℓ=1
1990	29	3	700.6	37.8	≤ -45	$\geq$99.9999	ℓ=1
1990	29	4	700.6	37.6	≤ -45	$\geq$99.9993	ℓ=1
1990	11	0	N/A	39.74	−13.96	99.91–99.95	ℓ=1, m=0
1990	11	1	700.6	38.09	−13.01	99.5–99.7	ℓ=1, m=0
1990	11	2	700.6	40.12	−10.26	93.8–96.5	ℓ=1, m=0
1990	11	3	700.6	41.64	−9.82	90.0–93.3	ℓ=1, m=0
1990	11	4	700.6	40.14	−8.46	84.7–90.0	ℓ=1, m=0
1994	26	0	N/A	38.14	−31.45	100	ℓ=1
1994	26	1	770.6	38.02	−35.29	100	ℓ=1
1994	26	2	770.6	38.02	−38.89	100	ℓ=1
1994	26	3	770.6	38.02	−39.64	99.999–100	ℓ=1
1994	26	4	770.6	37.73	−40.82	99.999	ℓ=1
1994	11	0	N/A	39.70	−9.08	98.5–99.0	ℓ=1, m=0
1994	11	1	770.6	39.73	−6.95	66.3–79.8	ℓ=1, m=0
1994	11	2	770.6	41.72	−5.73	50.0–59.5	ℓ=1, m=0
1994	11	3	770.6	40.46	−6.93	58.0–71.9	ℓ=1, m=0
1994	11	4	770.6	40.46	−7.22	75.4–84.7	ℓ=1, m=0

Over four runs, the WET consortium finds convincing evidence of a ∼38 s spacing in GD 358. The spacing's significance is difficult to recreate; in the worst case, the mode spacing from the 2000 campaign can only be matched by 0.003% of sets of random numbers and two of these runs produce a Q which is unattainable with one million random tests. The $m = 0$ modes alone are not uniquely spaced which implies that if trimmed modes lead to worse results, they should remain in the set.

4.3 BPM 37093

For the white dwarf BPM 37093, we use the fifteen modes adopted by Kanaan *et al.* (2005) for their model fits. The results in Table 4.6 are for the set of periods as well as their

Table 4.5 Comparing the Q statistic of the K–S test for the pulsation periods of GD 358 from 2000s WET runs reported by Kepler *et al.* (2003) or Provencal *et al.* (2009) with 10^6 sets of random numbers; period spacings tested from 5–50 s; 0–4 modes removed based on centering mode.

WET campaign	**#**	**−**	**center**	**best**	**log Q**	**percentile**	**notes**
2000	25	0	N/A	37.88	−23.00	99.997	ℓ=1
2000	25	1	704.2	37.95	−26.94	99.996–99.997	ℓ=1
2000	25	2	704.2	37.95	−22.55	99.94–99.96	ℓ=1
2000	25	3	704.2	37.95	−23.40	99.90–99.93	ℓ=1
2000	25	4	704.2	37.95	−22.11	99.64	ℓ=1
2000	25	1	771.2	37.94	−27.07	99.997–99.998	ℓ=1
2000	25	2	771.2	37.95	−32.56	99.998	ℓ=1
2000	25	3	771.2	37.95	−36.12	99.999	ℓ=1
2000	25	4	771.2	37.95	−40.85	99.999	ℓ=1
2000	14	0	N/A	40.81	−12.15	99.7–99.9	ℓ=1, m=0
2000	14	1	771.2	40.89	−12.05	98.7–99.0	ℓ=1, m=0
2000	14	2	771.2	40.89	−12.42	96.8–98.1	ℓ=1, m=0
2000	14	3	771.2	41.63	−10.55	90.0–92.0	ℓ=1, m=0
2000	14	4	771.2	40.72	−9.58	80.4–86.4	ℓ=1, m=0
2006	27	0	N/A	37.98	−31.44	≥99.9997	ℓ=1
2006	27	1	810.3	37.97	−31.08	≥99.999	ℓ=1
2006	27	2	810.3	37.84	−30.98	99.997	ℓ=1
2006	27	3	810.3	37.84	−30.79	99.991–99.993	ℓ=1
2006	27	4	810.3	37.97	−29.74	99.95–99.96	ℓ=1

corresponding frequencies. When all modes are considered, we find that the spacing between the published periods has a lower value of $\log Q$ than the spacing between the frequencies. Although the period spacing is more significant, it is only better than 96.6% of the random sets, so 30 000 sets out of one million sets of random numbers are able to have a spacing with a lower value of $\log Q$. When one of the periods is removed because its spacing with the 636.7 s mode is the worst of the set, the tests show a $\log Q$ in the 99^{th} percentile of the "stars" with randomly selected modes.

Table 4.6 Comparing the Q statistic of the K–S test for the fifteen pulsation modes of BPM 37093 as shown in Kanaan *et al.* (2005) with 10^6 sets of random numbers; period spacings tested from 5–50 s; frequency spacings tested from 5–100 μHz; 0–4 modes removed based on centering mode.

mode	**–**	**center**	**best**	**log Q**	**percentile**
period	0	N/A	16.90	−8.78	96.6–98.2
period	1	636.7	16.77	−13.55	99.2–99.6
period	2	636.7	16.76	−10.82	91.9–94.9
period	3	636.7	16.76	−10.17	86.8–90.0
period	4	636.7	16.76	−13.45	95.1–96.8
frequency	0	N/A	46.58	−6.23	87.1–90.0
frequency	1	1571	46.17	−7.05	81.6–89.1
frequency	2	1571	46.17	−6.00	50.0–59.6
frequency	3	1571	46.17	−5.79	36.9–50.0
frequency	4	1571	46.17	−8.74	70.2–78.1

4.4 PG 1219+534

We investigate varying asteroseismological results for the pulsating subdwarf B star PG 1219+534 (PG 1219). This sdB star is not a high-overtone pulsator and based on §1.2, it is not expected to exhibit equally spaced modes. Like BPM 37093, there is not a manifest spacing present between the periods or frequencies so we test both parameters. Charpinet *et al.* (2005) observe nine modes, including a tenth mode which lies barely above their lower threshold for detection. Reed *et al.* (2009) find a consistent detection of four modes, as well as the temporal appearance of three lower amplitude modes. The seven modes found by Reed *et al.* (2009) all have analogous results in Charpinet *et al.* (2005), so the similar results between the sets are not surprising.

Table 4.7 contains the frequency tests, while Table 4.8 displays the results of the period examinations. The Tables show the effects of including the weakly-detected tenth mode from Charpinet *et al.* (2005) and the three inconsistently observed modes from Reed *et al.* (2009). The modes with the highest amplitudes are selected as centering modes and are explicitly identified in the Tables.

The frequency tests find the best spacing at roughly 15.1 μHz, but the spacing never achieves

Table 4.7 Comparing the Q statistic of the K–S test for the pulsation frequencies of PG 1219+534, reported in either Charpinet *et al.* (2005) or Reed *et al.* (2009), with 10^6 sets of random numbers; 0–4 modes removed based on centering mode.

source	**#**	**−**	**center**	**range**	**best**	**log Q**	**percentile**
Charpinet	10	0	N/A	10–500 μHz	15.11	−7.34	94.2–97.2
Charpinet	10	1	7808	10–500 μHz	15.10	−11.60	98.4–99.0
Charpinet	9	0	N/A	10–500 μHz	13.29	−5.43	75.0–88.3
Charpinet	10	2	7808	10–500 μHz	15.06	−8.82	90.0–91.1
Charpinet	9	1	7808	10–500 μHz	15.06	−8.90	90.0–94.7
Charpinet	10	3	7808	10–500 μHz	15.12	−7.21	77.8–86.5
Charpinet	9	2	7808	10–500 μHz	15.06	−7.28	80.4–88.6
Reed	7	0	N/A	10–500 μHz	15.04	−5.67	76.3–89.9
Charpinet	10	4	7808	10–500 μHz	15.11	−6.64	69.3–82.2
Charpinet	9	3	7808	10–500 μHz	15.11	−5.39	53.9–71.3
Reed	7	1	6961	10–500 μHz	13.33	−3.99	11.5–34.2
Charpinet	9	4	7808	10–500 μHz	15.75	−3.78	14.0–37.0
Reed	7	2	6961	10–500 μHz	13.33	−4.42	50.0–64.8
Reed	7	3	6961	10–500 μHz	15.06	−4.10	65.7–90.0
Reed	4	0	N/A	10–500 μHz	26.57	−3.47	12.6–50.0

the 99^{th} percentile. Also, the range of the ten frequencies from Charpinet *et al.* (2005) is 6300 μHz; a spacing of less than 1% of the range should not be seriously considered when working with only ten modes. By excluding the tenth mode, thus reducing the range to 2400 μHz, the spacing only reaches the 90^{th} percentile when the lowest frequency is removed, but the spacing is still small compared to the range.

The period tests exhibit poor results for nearly every test except for a couple of instances when working with four modes. The lack of evidence supporting a significant spacing among the observed frequencies aligns with our expectations since low-overtone pulsations such as those we see in this subdwarf B star do not obey the asymptotic relation of equal mode spacings.

Since Charpinet *et al.* (2005) fit their stellar models to the individual frequencies, we also run a simulation similar to §2.6 by trying to match random numbers to each frequency or period. The results of these simulations, where 100 000 random sets are matched to the set of nine or ten observed modes, are printed in Table 4.9. The values of the raw χ^2 for the stellar model listed in the Table are calculated from the reported observed and theoretical modes.

Table 4.8 Comparing the Q statistic of the K–S test for the pulsation periods of PG 1219+534, reported in either Charpinet *et al.* (2005) or Reed *et al.* (2009), with 10^6 sets of random numbers; 0–4 modes removed based on centering mode.

mode	**#**	**−**	**center**	**range**	**best**	**log Q**	**percentile**
Charpinet	10	0	N/A	1–10 s	7.69	−2.67	0.612–17.5
Charpinet	10	1	128.1	1–10 s	7.81	−2.51	0.229–5.45
Charpinet	9	0	N/A	1–10 s	7.90	−2.20	0.543–16.7
Charpinet	10	2	128.1	1–10 s	7.68	−4.00	21.4–43.0
Charpinet	9	1	128.1	1–10 s	7.88	−1.83	0.0012–0.229
Charpinet	10	3	128.1	1–10 s	7.68	−3.70	13.1–30.7
Charpinet	9	2	128.1	1–10 s	7.88	−1.71	1.89–12.8
Reed	7	0	N/A	1–10 s	1.42	−2.91	0.606–15.5
Charpinet	10	4	128.1	1–10 s	7.88	−5.10	51.9–69.3
Charpinet	9	3	128.1	1–10 s	7.88	−3.65	13.5–33.0
Reed	7	1	143.7	1–10 s	1.45	−2.66	1.04–11.5
Charpinet	9	4	128.1	1–10 s	7.89	−3.51	14.0–37.0
Reed	7	2	143.7	1–10 s	1.42	−4.21	38.9–50.0
Reed	7	3	143.7	1–10 s	1.42	−4.81	99.0–99.9
Reed	4	0	N/A	1–10 s	5.24	−4.07	79.4–90.0

For both the nine-frequency set and the set of their corresponding periods, at least one of the random sets have a χ^2 better than the fitted model. Charpinet *et al.* (2005) choose the best nine modes from a set of twelve theoretical periods in their best stellar model. To simulate this selection, we find the nine random modes from a set of twelve which best fit the observed periods of PG 1219. We ignore the tenth mode because it is below the detection threshold. For 660 random sets out of 100 000 trials, the χ^2 is better than the best fitting published model.

4.5 PG 0014+067

The subdwarf B star PG 0014+067 (PG 0014) is first subjected to asteroseismological analysis from a single site by Brassard *et al.* (2001), while Vučković *et al.* (2006) present WET observations of the star. Although sdBs do not have a characteristic mode spacing, we test the identified periods and frequencies from each publication. The frequency results are in Table 4.10 while the period results can be found in Table 4.11.

Table 4.9 Fitting 10^5 sets of nine or ten random modes to the observed modes of PG 1219+534 from Charpinet *et al.* (2005). The number of modes and additional modes is shown. The χ^2 of the best fitting model from the same publication is compared to the best χ^2 of the simulated fits, and the reported model's percentile compared to the random sets is listed.

modes	**#**	**+**	**model**	**best**	**percentile**
frequencies	9	0	3.80×10^4	2.62×10^4	99.995
frequencies	10	0	5.02×10^4	3.13×10^5	100
periods	9	0	11.8	10.5	99.999
periods	10	0	12.4	43.3	100
periods	9	3	11.8	2.18	99.334

Brassard *et al.* (2001) identify thirteen modes above their amplitude threshold, and recognize ten additional low-amplitude modes when the optimal theoretical model is compared to the Fourier amplitude spectrum of the light curve of PG 0014. Table 4.10 and Table 4.11 present the K–S test results for both the 23- and 13-mode sets.

Like PG 1219, PG 0014 achieves a significance comparable to random numbers for both the sets of frequencies and periods. This is not a surprise since this sdB star only exhibits low-overtone pulsations and like PG 1219, no equal spacings are expected. This corroborates the model fit published in Brassard *et al.* (2001) where none of the modes are overtones with increasing n.

Since Brassard *et al.* (2001) fit their stellar models to the individual frequencies, we again run a simulation matching random numbers to each frequency or period and evaluating the χ^2 between the two sets. The results of these simulations, where 100 000 random sets are matched to the set of nine or ten observed modes, are printed in Table 4.12. The values of the raw χ^2 for the stellar model listed in the Table are calculated from the reported observed and theoretical modes.

The fitted model from Brassard *et al.* (2001) has a better χ^2 than any of the random sets when either 13 or 23 periods or frequencies are considered. We then simulate the selection of the thirteen best fitting modes from a set of 24 or 26 theoretical modes available in the range of observed periods of PG 0014. We ignore the ten modes that are below the detection

Table 4.10 Comparing the Q statistic of the K–S test for the pulsation frequencies of PG 0014+067, reported in either Vučković *et al.* (2006) or Brassard *et al.* (2001), with 10^6 sets of random numbers; 0–4 modes removed based on centering mode.

source	**#**	**−**	**center**	**range**	**best**	**log Q**	**percentile**
Vučković	12	0	N/A	20–200 μHz	87.91	−4.72	50.5–74.0
Brassard	13	0	N/A	60–700 μHz	66.46	−4.99	52.9–75.4
Brassard	23	0	N/A	60–700 μHz	65.79	−3.34	20.4–50.0
Brassard	13	1	6626	60–700 μHz	66.89	−3.81	6.44–25.6
Brassard	13	2	6626	60–700 μHz	66.48	−6.23	58.1–71.4
Brassard	13	3	6626	60–700 μHz	66.77	−5.19	37.6–50.0
Brassard	13	4	6626	60–700 μHz	66.77	−5.64	35.8–50.0
Brassard	23	1	6626	60–700 μHz	65.90	−3.96	11.9–33.4
Brassard	23	2	6626	60–700 μHz	65.90	−6.79	62.0–73.8
Brassard	23	3	6626	60–700 μHz	65.90	−7.67	64.8–73.8
Brassard	23	4	6626	60–700 μHz	65.90	−9.84	73.8–79.9
Vučković	12	1	7089	20–200 μHz	87.82	−5.09	47.7–50.0
Vučković	12	2	7089	20–200 μHz	85.73	−4.10	21.6–41.1
Vučković	12	3	7089	20–200 μHz	87.06	−3.65	5.38–19.9
Vučković	12	4	7089	20–200 μHz	90.65	−2.78	0.916–5.09

threshold. When we ignore 11 random modes, over 6% of the random sets are a better fit to the observations than the best theoretically derived modes. When there are 26 numbers in the pool of random modes, over 10% of the random sets produce a χ^2 lower than the best fitting stellar model. If there is over a 10% chance such a fit can be produced by numbers with no physical constraints, the best fitting model by Brassard *et al.* (2001) does not appear to be very significant.

Table 4.11 Comparing the Q statistic of the K–S test for the pulsation periods of PG 0014+067, reported in either Vučković *et al.* (2006) or Brassard *et al.* (2001), with 10^6 sets of random numbers; 0–4 modes removed based on centering mode.

source	**#**	**−**	**center**	**range**	**best**	**log Q**	**percentile**
Vučković	12	0	N/A	1–10 s	2.28	−4.51	50.5–74.0
Brassard	13	0	N/A	0.5–15 s	0.979	−4.58	52.9–75.4
Brassard	23	0	N/A	0.5–15 s	0.720	−3.46	20.4–50.0
Vučković	12	1	141.1	1–10 s	2.32	−4.91	25.0–47.7
Vučković	12	2	141.1	1–10 s	2.32	−4.84	21.6–41.1
Vučković	12	3	141.1	1–10 s	2.25	−4.59	19.9–38.5
Vučković	12	4	141.1	1–10 s	2.32	−5.81	50.0–54.9
Brassard	13	1	150.9	0.5–15 s	0.980	−3.65	6.44–25.6
Brassard	13	2	150.9	0.5–15 s	0.980	−4.20	21.9–40.7
Brassard	13	3	150.9	0.5–15 s	0.980	−2.88	0.793–5.71
Brassard	13	4	150.9	0.5–15 s	0.983	−2.41	0.982–5.39
Brassard	23	1	150.9	0.5–15 s	0.849	−3.38	11.9–33.4
Brassard	23	2	150.9	0.5–15 s	0.849	−3.51	13.1–30.1
Brassard	23	3	150.9	0.5–15 s	0.849	−3.22	14.2–28.8
Brassard	23	4	150.9	0.5–15 s	0.740	−3.39	14.9–27.7

Table 4.12 Fitting 10^5 sets of 13 or 23 random modes to the observed modes of PG 0014+067 from Brassard *et al.* (2001). The number of modes and additional modes is shown. The χ^2 of the best fitting model from the same publication is compared to the best χ^2 of the simulated fits, and the reported model's percentile compared to the random sets is listed.

modes	**#**	**+**	**model**	**best**	**percentile**
frequencies	13	0	1.09×10^5	3.77×10^5	100
frequencies	23	0	1.28×10^5	4.35×10^5	100
periods	13	0	33.2	61.0	100
periods	23	0	34.9	92.7	100
periods	13	11	33.2	6.17	93.9
periods	13	13	33.2	5.60	89.9

4.6 η Boötis

As stated in §2.1, Guenther *et al.* (2005) identify dozens of spectrum peaks in the *MOST* observations of η Boo as possible pulsation modes. They pare down the selection further by identifying the peaks which line up well on an échelle diagram with a folding frequency of $40\,\mu$Hz. This results in 15 peaks spaced by $\sim 40\,\mu$Hz, including five modes which may be part of two multiplets. Guenther *et al.* (2005) include an additional eight frequencies identified by Kjeldsen *et al.* (2003) and after removing two overlapping modes between the independent results, they craft a list of 21 well-spaced modes.

We consider a number of combinations of those 21 modes. Table 4.13 contains the results for the *MOST* modes labeled 3–10 along with separate tests for the eight modes incorporated from Kjeldsen *et al.* (2003). The centering modes chosen from each data set are the highest amplitude modes from observation. Both sets remain in the 90^{th} percentile from eight to four modes so they compare well with sets of eight randomly selected numbers. However, a couple of random sets are on par with the *MOST* and Kjeldsen modes.

Table 4.13 Comparing the Q statistic of the K–S test for eight pulsation frequencies of η Boötis, reported in Guenther *et al.* (2005) and Kjeldsen *et al.* (2003), with 10^6 sets of random numbers; frequency spacings tested from 5–50 μHz; 0–4 modes removed based on centering mode.

source	**−**	**center**	**best**	**log Q**	**percentile**
Guenther	0	N/A	41.24	−17.15	≥99.9997
Guenther	1	492.9	40.85	−14.56	99.990–99.997
Guenther	2	492.9	40.86	−10.47	99.0–99.9
Guenther	3	492.9	40.43	−7.56	95.3–99.0
Guenther	4	492.9	40.06	−4.60	90.0–99.0
Kjeldsen	0	N/A	40.77	−17.64	≥99.9997
Kjeldsen	1	853.6	40.94	−15.07	≥99.997
Kjeldsen	2	853.6	40.94	−11.10	99.0–99.9
Kjeldsen	3	853.6	40.92	−7.82	99.0–99.9
Kjeldsen	4	853.6	40.79	−4.77	99.0–99.9

When faced with options for *MOST* modes 1 and 2, Guenther *et al.* (2005) elect to test the second mode in each "multiplet." Table 4.14 details the performance of ten modes against

random selections with all combinations of the "multiplets" under consideration. Compared to the eight modes in Table 4.13, the best ten-mode spacings have slightly higher frequencies for five out of the six combinations, although the other combination, *MOST* modes 1c and 2b, has the lowest value of Q.

Table 4.15 shows how well *MOST* modes 3–10 perform in tandem with the eight Kjeldsen frequencies. Because of the way Guenther *et al.* (2005) select these modes, the additional numbers greatly bolster the K–S test results by outstripping all or most of the random spacings. Since the significances decline when frequencies are removed, even the worst fitting modes can be considered essential to the overall spacing.

Subsequent tests examine combinations of frequencies which are not tested in Guenther *et al.* (2005). The additional combinations highlight the contributions of certain groups of modes. In lieu of *MOST* modes 11 and 12, Guenther *et al.* (2005) elect to use the corresponding frequencies identified in Kjeldsen *et al.* (2003). Table 4.16 contains the results for the K–S test for *MOST* modes 3–12, allowing for a direct comparison between modes 11 and 12 and the candidates for modes 1 and 2 shown in Table 4.14. While modes 3–12 still perform very well, most combinations of modes 1–10 fare better against the random sets.

Table 4.17 displays the test of twelve *MOST* frequencies which includes any combination of the "multiplets" of modes 1 and 2. As seen in prior tests, if we add k modes to a set of N well-spaced modes, where the additional k modes are also well-spaced with the original set of N, the set of $N + k$ modes have a lower value of $\log Q$ than the set of N. The larger set of $N + k$ modes also improve in comparison to random modes, and the twelve here perform better than any of the ten seen in Table 4.14 or Table 4.16. However, the 39 μHz spacing favored by modes 11 and 12 continues here as opposed to the optimal 41 μHz spacings with modes 1 and 2. At the same time, the set containing modes 1c and 2b again has the best results overall.

Table 4.14 Comparing the Q statistic of the K–S test for ten pulsation frequencies of η Boötis, denoted as *MOST* modes 3–10 and one mode from each of the "multiplets" 1 and 2, as reported in Guenther *et al.* (2005), with 10^6 sets of random numbers; frequency spacings tested from 5–50 μHz; 0–4 modes removed based on the 492.9 μHz centering mode.

1, 2	**–**	**best**	**log Q**	**percentile**
a, a	0	41.85	−20.26	99.9996–99.9998
a, a	1	41.77	−18.29	99.991–99.997
a, a	2	41.34	−16.58	99.96–99.98
a, a	3	40.83	−14.67	99.90–99.98
a, a	4	40.82	−10.57	99.0–99.7
a, b	0	41.26	−19.93	99.9993–99.9996
a, b	1	41.40	−19.34	99.997–99.998
a, b	2	41.40	−16.23	99.96–99.98
a, b	3	41.33	−13.05	99.7–99.9
a, b	4	41.11	−9.93	95.9–98.5
b, b	0	41.12	−22.54	≥99.9998
b, b	1	41.34	−21.28	≥99.9996
b, b	2	41.12	−17.98	99.990–99.995
b, b	3	41.12	−13.84	99.7–99.9
b, b	4	40.85	−10.51	99.0–99.7
b, a	0	41.12	−20.57	99.9996–99.9998
b, a	1	41.34	−21.25	≥99.9996
b, a	2	41.34	−17.37	99.990
b, a	3	41.26	−13.31	99.7–99.9
b, a	4	41.01	−10.13	99.0–99.7
c, a	0	41.46	−21.30	≥99.9998
c, a	1	41.36	−19.68	99.997–99.998
c, a	2	41.36	−16.47	99.96–99.98
c, a	3	41.28	−13.24	99.7–99.9
c, a	4	40.88	−10.44	99.0–99.7
c, b	0	40.88	−26.48	100
c, b	1	40.97	−22.35	≥99.9996
c, b	2	40.92	−19.08	99.998–99.999
c, b	3	40.92	−14.60	99.90–99.98
c, b	4	40.94	−10.31	99.0–99.7

Table 4.15 Comparing the Q statistic of the K–S test for sixteen pulsation frequencies of η Boötis, reported in Guenther *et al.* (2005) and Kjeldsen *et al.* (2003), with 10^6 sets of random numbers; frequency spacings tested from 5–50 μHz; 0–4 modes removed based on the centering mode.

–	**center**	**best**	**log Q**	**percentile**
0	N/A	39.68	≤ -45	100
1	492.9	40.60	-44.15	100
2	492.9	40.71	-42.34	100
3	492.9	40.64	-36.28	100
4	492.9	40.70	-32.20	$\geq$99.99
1	853.6	40.62	-43.38	100
2	853.6	39.54	-38.90	100
3	853.6	39.51	-34.31	$\geq$99.9999
4	853.6	39.35	-28.85	$\geq$99.99

Table 4.16 Comparing the Q statistic of the K–S test for the *MOST* frequencies 3–12 of η Boötis, as reported in Guenther *et al.* (2005), with 10^6 sets of random numbers; frequency spacings tested from 5–50 μHz; 0–4 modes removed based on the 492.9 μHz centering mode.

–	**best**	**log Q**	**percentile**
0	39.23	-20.03	99.9996–99.9998
1	39.19	-18.45	99.991–99.997
2	39.09	-15.36	99.90–99.96
3	40.05	-13.01	99.7–99.9
4	40.02	-10.40	99.0–99.7

Table 4.17 Comparing the Q statistic of the K–S test for twelve pulsation frequencies of η Boötis, denoted as *MOST* modes 3–12 and one mode from each of the "multiplets" 1 and 2, as reported in Guenther *et al.* (2005), with 10^6 sets of random numbers; frequency spacings tested from 5–50 μHz; 0–4 modes removed based on the 492.9 μHz centering mode.

1, 2	**–**	**best**	**log Q**	**percentile**
a, a	0	39.18	−20.65	99.999
a, a	1	39.29	−21.55	≥99.995
a, a	2	39.20	−20.92	99.990–99.993
a, a	3	39.20	−18.50	99.94–99.98
a, a	4	39.10	−15.45	99.6–99.8
a, b	0	39.18	−22.97	100
a, b	1	39.20	−26.07	≥99.995
a, b	2	39.20	−20.92	99.990–99.993
a, b	3	39.20	−18.50	99.94–99.98
a, b	4	39.10	−15.45	99.6–99.8
b, a	0	39.09	−21.85	≥99.999
b, a	1	39.27	−21.15	≥99.995
b, a	2	39.30	−21.27	99.993–99.997
b, a	3	39.20	−18.52	99.94–99.98
b, a	4	39.11	−15.59	99.6–99.8
b, b	0	39.09	−23.01	100
b, b	1	39.18	−25.65	≥99.995
b, b	2	39.30	−21.27	99.993–99.997
b, b	3	39.20	−18.52	99.94–99.98
b, b	4	39.11	−15.59	99.6–99.8
c, a	0	39.29	−25.51	100
c, a	1	39.27	−24.78	≥99.995
c, a	2	39.29	−21.00	99.993
c, a	3	39.09	−18.54	99.94–99.98
c, a	4	39.10	−15.48	99.6–99.8
c, b	0	39.29	−29.85	100
c, b	1	39.19	−25.78	≥99.995
c, b	2	40.59	−22.18	99.997–99.999
c, b	3	39.09	−18.54	99.94–99.98
c, b	4	39.10	−15.48	99.6–99.8

As discussed in § 3.4 and § 4.2, the presence of rotationally split multiplets or just modes in close proximity can easily enhance the significance of a set of modes. The next round of tests include the triplet of *MOST* mode 1 and the doublet of mode 2 with modes 3–10 and the results are shown in Table 4.18. As seen with PG 1159 and GD 358, the Q for this set of frequencies bests every or nearly every random set. Interestingly, the preferred spacing fluctuates greatly after excising the first two modes, which are modes 1a and 1b, in that order. Those modes are 4.5 and 3.2μHz less than mode 1c, respectively, and excluding those modes results in increasing the significance of spacings between the remaining modes and 1c. While their relative locations seem to favor longer spacings, the spacing between 1a or 1b and 2a may shorten the most prominent spacing.

Table 4.18 Comparing the Q statistic of the K–S test for thirteen pulsation frequencies of η Boötis, reported in Guenther *et al.* (2005), with 10^6 sets of random numbers; frequency spacings tested from 5–50 μHz; 0–4 modes removed based on the 492.9 μHz centering mode.

–	**best**	**log Q**	**percentile**
0	40.13	−31.67	100
1	39.88	−29.48	≥99.991
2	41.03	−25.03	99.9991–99.9998
3	40.96	−26.71	100
4	40.82	−22.96	≥99.992

Table 4.19 shows the results for all the *MOST* modes identified by Guenther *et al.* (2005). The inclusion of modes 11 and 12 influences a shorter spacing than those seen in Table 4.18 and the additional modes boost the value of log Q as suspected. While the unique shifts are easier to see by going from thirteen to fifteen modes, comparing these values to those of modes 3–12 in Table 4.16 are more difficult. The candidate modes 1 and 2 constitute a fifty percent increase in modes which causes a dramatic shift in Q, although apparently less of a change in frequency for the best spacing.

Expanding on the results for the sixteen-mode sets seen in Table 4.15, *MOST* modes 1b and 2b are included in the next round of tests shown in Table 4.20. Together, those eighteen modes achieve results that can not be matched by an equal set of random numbers.

Table 4.19 Comparing the Q statistic of the K–S test for fifteen pulsation frequencies of η Boötis, reported in Guenther *et al.* (2005), with 10^6 sets of random numbers; frequency spacings tested from 5–50 μHz; 0–4 modes removed based on the 492.9 μHz centering mode.

–	**best**	**log Q**	**percentile**
0	39.55	−35.89	100
1	39.35	−33.75	100
2	39.36	−29.57	99.9997–99.9998
3	39.36	−29.32	≥99.99
4	39.21	−26.24	≥99.99

Table 4.20 Comparing the Q statistic of the K–S test for eighteen pulsation frequencies of η Boötis, reported in Guenther *et al.* (2005), with 10^6 sets of random numbers; frequency spacings tested from 5–50 μHz; 0–4 modes removed based on centering mode.

–	**center**	**best**	**log Q**	**percentile**
0	N/A	39.6	≤ −45	100
1	492.9	39.7	≤ −45	100
2	492.9	40.6	≤ −45	100
3	492.9	40.48	−44.25	100
4	492.9	40.48	−42.17	100
1	853.6	40.6	≤ −45	100
2	853.6	40.6	≤ −45	100
3	853.6	39.53	−43.70	100
4	853.6	39.51	−38.66	100

All 21 frequencies, including the multiplets and following the practice by Guenther *et al.* (2005) of favoring the modes in Kjeldsen *et al.* (2003) over *MOST* modes 11 and 12, are brought together for the last round of tests. The results are found in Table 4.21. The program's calculated Q literally bottomed out with all of the well-matched numbers by forming a plateau (or plateaus) of highest possible significances in all the possible tests.

In order to restore proper objectivity into testing the reported spacings of η Boötis, the number of significant frequency peaks observed must be considered. Recall in §2.1 that Guenther *et al.* (2005) set up a scheme to choose modes for their model fits by eliminating equally significant modes from the *MOST* observations because they do not adhere to the scheme. In

Table 4.21 Comparing the Q statistic of the K–S test for 21 pulsation frequencies of η Boötis, reported in Guenther *et al.* (2005) and Kjeldsen *et al.* (2003), with 10^6 sets of random numbers; frequency spacings tested from 5–50 μHz; 0–4 modes removed based on centering mode.

–	**center**	**best**	**log Q**	**percentile**
0	N/A	39.6	≤ -45	100
1	492.9	39.6	≤ -45	100
2	492.9	39.6	≤ -45	100
3	492.9	40.6	≤ -45	100
4	492.9	39.6	≤ -45	100
1	853.6	39.65	≤ -45	100
2	853.6	40.65	≤ -45	100
3	853.6	40.6	≤ -45	100
4	853.6	40.65	≤ -45	100

the case of Kjeldsen *et al.* (2003), eight modes are selected from 21 observed, while Guenther *et al.* (2005) use ∼70 peaks of varying strength to find fifteen modes of which either eight or ten are tested at a time. Since the previous Tables use groupings of twelve, thirteen, and fifteen modes, Table 4.22 shows how well those sets compare to a selection from a pool of 70 random numbers as well as the ability to find eight well-spaced modes out of 21. All combinations of the multiplets are considered in the sets and the frequencies from Guenther *et al.* (2005) are not incorporated with the modes from Kjeldsen *et al.* (2003).

Although the significances always increase with additional numbers, *MOST* modes 11 and 12 now hinder the percentile compared to random sets. Modes 1c and 2b perform the best out of the multiplets, which follows from their ability to line up better with modes 3–10 on the échelle diagram in Figure 2.2 than the other multiplets. Their relative prominence is previously addressed in Tables 4.14 and 4.17.

When all the multiplets are included in the set, the poor performance of certain modes, e.g. 1a, lead the thirteen-mode set to falter against random sets with a surfeit of options despite decreasing Q fourteen orders of magnitude from the eight-mode test. Knowing that the successful results published by Guenther *et al.* (2005) are reproducible by a significant proportion of equally sized sets composed of random numbers, we may question the legitimacy

Table 4.22 Comparing the Q statistic of the K–S test for a varying number of pulsation frequencies of η Boötis, with ∼70 reported in Guenther *et al.* (2005) and 21 presented in Kjeldsen *et al.* (2003), against 10^6 sets of an equal amount of random numbers; frequency spacings tested from 5–50 μHz; 55–62 (Guenther) or 13 (Kjeldsen) modes removed based on centering mode at 492.9 μHz (Guenther) or 853.6 μHz (Kjeldsen).

N	−	**best**	**log Q**	**percentile**	**notes**
15	55	39.55	−35.89	80.6–83.5	1, 2, 3–10, 11, 12
13	57	40.13	−31.67	86.0–89.0	1, 2, 3–10
12	58	39.18	−20.65	32.6–38.4	1a, 2a, 3–10, 11, 12
12	58	39.18	−22.97	50.0–50.8	1a, 2b, 3–10, 11, 12
12	58	39.09	−21.85	38.4–44.4	1b, 2a, 3–10, 11, 12
12	58	39.09	−23.01	50.8–57.1	1b, 2b, 3–10, 11, 12
12	58	39.29	−25.51	63.3–69.3	1c, 2a, 3–10, 11, 12
12	58	39.29	−29.85	84.4–88.2	1c, 2b, 3–10, 11, 12
10	60	41.85	−20.26	74.2–80.9	1a, 2a, 3–10
10	60	41.26	−19.93	66.6–74.2	1a, 2b, 3–10
10	60	41.12	−20.57	74.2–80.9	1b, 2a, 3–10
10	60	41.12	−22.54	86.5–90.0	1b, 2b, 3–10
10	60	41.46	−21.30	80.9–86.5	1c, 2a, 3–10
10	60	40.88	−26.48	98.0–99.0	1c, 2b, 3–10
10	60	39.23	−20.03	74.2–80.9	3–10, 11, 12
8	62	41.24	−17.15	92.5–96.4	3–10
8	13	40.77	−17.64	99.6–99.8	Kjeldsen

of the reported 40 μHz spacing and its role in modeling the interior of η Boötis. From our results, we can say their method of considering less than a quarter of the modes identified from observations ensures them a promising spacing, and their χ^2 test gives them a quantifiable significance lacking a basis for comparison.

The eight modes from Kjeldsen *et al.* (2003) look much better against random comparisons than the *MOST* modes since they are selected from 21 modes of significance.

CHAPTER 5. SUMMARY AND CONCLUSION

Recognizing that verified mode spacings in pulsating stars are useful in narrowing down parameters in stellar models, researchers present a number of techniques to judge their observations. However, the statistical methods only use numbers which are subject to users' selection biases. Since the methods treat all numbers equally, the statistics require an additional objective tool.

In an attempt to replicate the results reported in Guenther *et al.* (2005), we use a random number generator to create sets of numbers and matching a simulated "observed" set to a slate of stellar "models." We also evaluate the match using the χ^2, and find the random numbers could not approach the proximity found between η Boötis and models. However, the χ^2 distribution resembles a log-normal distribution, so we evaluate that claim with a Kolmogorov-Smirnov Test. Since that test has promising results, we repeat the test for other "observed" sets to see if an analytic solution to the distribution exists for all sets. We find that the distributions are found numerically rather than analytically; the composition of each "observed" set affects their associated distribution of χ^2. The shape of these distributions may be compared to distributions derived from well-spaced numbers, especially those found from observations.

We use the random number generator with another technique: the significance, Q, of the K–S test. As Kawaler (1988) uses with observations of PG 1159–035, we run the K–S test on sets of random numbers to set an objective gauge on the verisimilitude of reported spacings. We set up a table to compare future results to 10^6 sets of eight to twelve random numbers. With more prolific results, e.g. the dozens of modes detected in the WET target stars and η Boötis, additional simulations are necessary but attainable. These simulations

allow asteroseismologists to judge the best mode spacing with no omissions by showing the likelihood of reproducing spacings of comparable strength with random numbers.

Although the program exhibits a strong bias for several observed modes, it can still serve as a helpful tool to impartially identify and assess the strength of potential mode spacings. The program allows users to better remove bias by showing the likelihood of finding well-aligned modes. Using the program on more stars known to have observable spacings further calibrates how the percentiles should be interpreted.

The inverse variance test, an alternative method to the K-S test developed by O'Donoghue (1994), may also be applied when examining random "stars." The significance statistic of the K–S test displays a bifurcation in stronger spacings. Since this flaw is not present in the inverse variance test, it may be more effective to find random spacings with that technique.

By setting benchmarks on perceived spacings, we incorporate a degree of statistical uncertainty to these results. The tests themselves are not definitive by nature; dimensionless measurements only make sense through comparison. If future research applies similar work to analyzing prospective spacings, the publications would enhance the quantitative element of the language used to describe such spacings.

BIBLIOGRAPHY

Bedding, T. R., and Kjeldsen, H. 2010. Scaled oscillation frequencies and échelle diagrams as a tool for comparative asteroseismology. *Communications in Asteroseismology*, *161*, 3-15.

Brassard, P., *et al.* 2001. Discovery and asteroseismological analysis of the pulsating sdB star PG 0014+067. *Astrophysical Journal*, *563*, 1013-1030.

Brown, T. M. and Gilliland, R. L. 1994. Asteroseismology. *Annual Review of Astronomy and Astrophysics*, *32*, 37-82.

Charpinet, S., *et al.* 2005. Structural parameters of the hot pulsating B subdwarf PG 1219+534 from asteroseismology. *Astronomy and Astrophysics*, *437*, 575-597.

Christensen-Dalsgaard, J. 2002. Helioseismology. *Reviews of Modern Physics*, *74*, 1073-1129.

Christensen-Dalsgaard, J. 2003. *Lecture Notes on Stellar Oscillations*, 5th edition, `http://users-phys.au.dk/jcd/oscilnotes/`, University of Aarhus.

Christensen-Dalsgaard, J. and Pérez Hernández, F. 1992. The phase function for stellar acoustic oscillations. I - Theory. *Monthly Notices of the Royal Astronomical Society*, *257*, 62-88.

Christensen-Dalsgaard, J., Gough, D., and Toomre, J. 2002. Seismology of the sun. *Science*, *229*, 923-931.

Duvall, T. L. Jr., *et al.* 1988. Frequencies of solar p-mode oscillations. *Astrophysical Journal*, *324*, 1158-1171.

Gautschy, A. and Saio, H. 1995. Stellar pulsations across the HR diagram: part 1. *Annual Review of Astronomy and Astrophysics*, *33*, 75-113.

Gilliland, R., *et al.* 2010. Kepler asteroseismology program: introduction and first results. *Publications of the Astronomical Society of the Pacific*, *122*, 131-143.

Grec, G., Fossat, E. and Pomerantz, M. A. 1983. Full-disk observations of solar oscillations from the geographic south pole: latest results. *Solar Physics*, *82*, 55-66.

Guenther, D. B. and Brown, K. I. T. 2005. Matching stellar models to oscillation data. *Astrophysical Journal*, *600*, 419-434.

Guenther, D. B., *et al.* 2005. Stellar model analysis of the oscillation spectrum of η Boötis obtained from *MOST*. *Astrophysical Journal*, *635*, 547-559.

Hansen, C. J., Kawaler, S. D. and Trimble, V. 2004. *Stellar Interiors*, 2nd edition, Springer-Verlag.

Kanaan, A., *et al.* 2005. Whole Earth Telescope observations of BPM 37093: A seismological test of crystallization theory in white dwarfs. *Astronomy and Astrophysics*, *432*, 219–224.

Kawaler, S. D. 1988. The stellar seismology of the hot white dwarf star PG 1159–035. *IAU Symposium 123, Advances in Helio- and Asteroseismology*, 329-332, eds. Christensen-Dalsgard, J. & Frandsen, S., Reidel, Dordrecht.

Kepler, S. O., *et al.* 2003. The everchanging pulsating white dwarf GD 358. *Astronomy and Astrophysics*, *401*, 639-654.

Kernighan, B. W. and Ritchie, D. 1988. *The C Programming Language*, 2nd edition, Prentice Hall.

Kjeldsen, H., *et al.* 2003. Confirmation of solar-like oscillations in η Boötis. *Astronomical Journal*, *126*, 1483-1488.

Koch, D., *et al.* 2010. Kepler mission design, realized photometric performance, and early science. *Astrophysical Journal*, *713*, L79-L86.

Libbrecht, K. G. 1988. Solar and stellar seismology. *Space Science Reviews*, *47*, 275-301.

O'Donoghue, D. 1994. The inverse variance method for assessing measurements of dP/dt and equal-period spacings in rapid variable stars. *Monthly Notices of the Royal Astronomical Society*, *270*, 222-228.

Press, W., *et al.* 1992. *Numerical Recipes in C: The Art of Scientific Computing*, 2nd edition, Cambridge University Press.

Provencal, J. L., *et al.* 2009. 2006 Whole Earth Telescope observations of GD358: a new look at the prototype DBV. *Astrophysical Journal*, *693*, 564-585.

Reed, M. D., *et al.* 2009. Time-series spectroscopy and photometry of the pulsating subdwarf B star PG 1219+534 (KY UMa). *Astronomy and Astrophysics*, *493*, 175-183.

Reed, M. D., *et al.* 2010. First *Kepler* results on compact pulsators - III. Subdwarf B stars with V1093 Her and hybrid (DW Lyn) type pulsations. *Monthly Notices of the Royal Astronomical Society*, *409*, 1496-1508.

Tassoul, M., 1980. Asymptotic approximations for stellar nonradial pulsations. *Astrophysical Journal Supplement Series*, *43*, 469-490.

Vučković, M., *et al.* 2006. Whole Earth Telescope observations of the pulsating subdwarf B star PG 0014+067. *Astrophysical Journal*, *646*, 1230-1240.

Vuille, F., *et al.* 2000. Normal modes and discovery of high-order cross-frequencies in the DBV white dwarf GD 358. *Monthly Notices of the Royal Astronomical Society*, *314*, 689-701.

Winget, D. E., *et al.* 1985. A measurement of secular evolution in the pre-white dwarf star PG 1159–035. *Astrophysical Journal*, *292*, 606-613.

Winget, D. E., *et al.* 1991. Asteroseismology of the DOV star PG1159–035 with the Whole Earth Telescope. *Astrophysical Journal*, *378*, 326-346.

Winget, D. E., *et al.* 1994. Whole Earth Telescope observations of the DBV white dwarf GD 358. *Astrophysical Journal*, *430*, 839-849.